An-Najah National University

Faculty of Graduate Studies

Effect of Applied Fields on The Magnetic Properties of Donor Impurity Confined in Parabolic GaAs Quantum Dot

By

Amal Jawdat Nayef Darawsheh

Supervisor

Prof. Mohammad Elsaid

This Thesis is Submitted in partial Fulfillment of the Requirements for the Degree of Master in Physics, Faculty of Graduate Studies, An-Najah National University, Nablus-Palestine

2018

Effect of Applied Fields on The Magnetic Properties of Donor Impurity Confined in Parabolic GaAs Quantum Dot

By

Amal Jawdat Nayef Darawsheh

This thesis was defended successfully on 12/6/2018 and approved by:

Defense committee Members	**Signature**
- Prof. Mohammad Elsaid / Supervisor	**……**
- Dr. Muayad Abu Saa / External Examiner	**……**
- Dr. Mohammed Abu-Jafar / Internal Examiner	**……**

Dedicated

My dearest husband, who leads me through the valley of

darkness with light of hope and support

My Mother and my Father

My kids: Oday, and Sham

My Brothers and Sisters

Acknowledgements

I would like to express my sincere gratitude to those who gave me the assistance and support during my master study especially my husband Ahmed.

My deepest gratitude and appreciation goes to my supervisor prof. Mohammad Elsaid, and Mr. Ayham Elshaer for their continuous support

and advice at all stages of my work.

Another word of special thanks goes to An-Najah National University, especially for all those in the Faculty of Graduate Studies / Physics Program.

Finally, a thank from my heart to my parents for their great support, to my lovely kids (Oday and Sham), and to my brothers and sisters

الاقرار

أنا الموقعة أدناه مقدمة الرسالة التي تحمل عنوان:

Effect of Applied Fields on The Magnetic Properties of Donor Impurity Confined in Parabolic GaAs Quantum Dot

أقر بأن ما اشتملت عليه هذه الرسالة، انما هي نتاج جهدي الخاص، باستثناء ما تمت الاشارة اليه حيثما ورد، وأن هذه الرسالة ككل، أو أي جزء منها لم يقدم لنيل أي درجة علمية، أو بحث علمي أو بحثي لدى أي مؤسسة تعليمية أو بحثية أخرى.

Declaration

The work provided in this Thesis, unless otherwise referenced, is the researchers own work, and has not been submitted elsewhere for any other degree or qualification.

Student's name: **اسم الطالبة:**

Signature: **التوقيع:**

Date: **التاريخ:**

Table of Contents

List of Tables

List of Figure

List Of Abbreviations

QD	Quantum Dot
QW	Quantum Well
QWW	Quantum Well Wire
GaAs	Gallium Arsenide
AlGaAs	Aluminum Gallium Arsenide
EMA	Effective Mass Approximation
RSOI	Rashba Spin Orbit Interaction
DOS	Density Of States
EDM	Exact Diagonalization Method
SET	Single Electron Transistor
FEM	Finite Element Method
PMM	Potential Morphing Method
3D	Three Dimension
2D	Tow Dimension
1D	One Dimension
0D	Zero Dimension
M	Magnetization
χ	Susceptibility
$C_{\boldsymbol{\nu}}$	Heat Capacity
α	RSOI coupling factor
ω_{eff}	Effective frequency
ω_c	Cyclotron frequency
ω_0	Confining frequency
B	Magnetic Field
F	Electric Field
e	charge of electron
m_0	Mass of electron
m^*	Effective mass of electron
meV	milli electron Volt
P	Linear momentum
A	Vector potential
c	Speed of light
i	Imaginary number
T	Temperature
K	Kelvin degree
nm	nano meter
K_B	Boltzmann constant
n	Radial quantum number
m	Magnetic quantum number
R^*	Effective Rydberg energy unit

a^*	Effective Bohr radius
$\hbar$	Reduced Blank's constant
ϵ	Dielectric constant of material
Ψ	Wave function

Effect of Applied Fields on The Magnetic Properties of Donor Impurity Confined in Parabolic GaAs Quantum Dot

By
Amal Jawdat DARAWSHEH
Supervisor
Prof. Mohammad Elsaid

Abstract

Based on the effective mass approximation, the magnetic properties of parabolic GaAs quantum dot have been investigated in the presence of magnetic field, tilted electric field, in addition to Rashba Spin Orbit Interaction. The exact diagonalization method is used to solve the Hamiltonian of donor impurity confined in a Quantum Dot (QD) and to obtain the Eigen energies. The Binding energy of the donor impurity has been calculated as a function of various QD physical parameters.

We have shown the dependence of the magnetic quantities like: magnetization (M) magnetic susceptibility (χ) and heat capacity (C_{ν}) of the donor impurity in the QD on: both magnetic and external electric fields, confining frequency (ω_0), titled angle (θ), and temperature (T).

Furthermore, the effects of Rashba Spin- Orbit Interaction term, as a key parameter in the field of Spintronics, on the magnetic properties has also been studied.

The results reveal that the external electric field strength and its tilt angle, magnetic field, temperature, confining frequency, in addition to Rashba effect affect the magnetic properties of the QD, changing it from

diamagnetic to paramagnetic material. Also, the heat capacity of the QD is affected by those parameters.

Our results are in very good quantitively agreement with the corresponding ones reported in the literature.

Chapter 1
Introduction

Technological development requires smaller and faster machines. So, Nanoscience became a rich field for researchers; to study the electronic, magnetic, optical and thermodynamic properties of low-dimensional Nanostructures.

1.1 Nanostructures

Low dimensional semiconductors or nanostructure semiconductors are those which have at least one dimension in nanoscale, Nanoscale means a range from 0 to 100 Nanometers (nm). Depending on the number of electrons that can move freely in dimensions, nanostructures are classified into three categories:

1. Quantum Well (QW): in those heterostructures, electrons are trapped in one dimension, and free to move in two dimensions (2D).

2. Quantum Well Wire (QWW): the electrons are free to move in one dimension and confined in the two other dimensions (1D).

3. Quantum Dot (QD): electrons are confined in all three dimensions (0D) [1].

The confinement phenomena change the density of states of the nanostructure [2] as shown in figure 1.1, and hence, the energy spectra are affected.

1.2 QD Heterostructure

In QD, since the electrons are trapped in the three spatial dimensions, the energy spectra are significantly affected, and shows a discrete behavior like the real atoms, so that they are called artificial atoms, Figure (1.2) shows the similarity of the electronic energy levels for both real atoms and

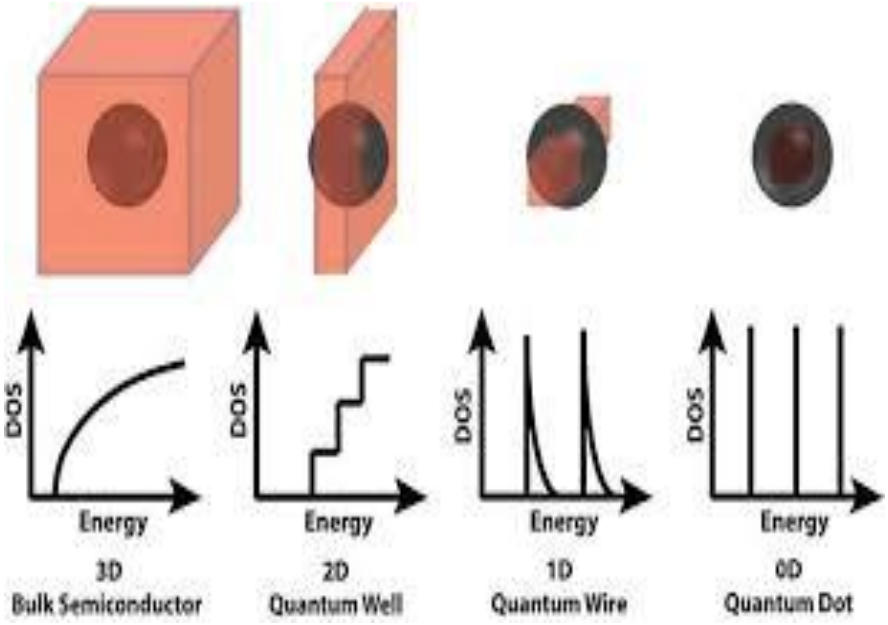

Figure 1.1: Density of states for bulk materials (3D), QW (2D), QWW (1D). and QD(0D) [54].

QD. However, there is a unique and supreme advantage of QD over real atoms, that their energy levels can be modulated and manipulated by different methods [3], such as changing the size and shape of the QD, and

this occurs during fabrication processes. Fabrication of QD can be made by different methods, such as: Colloidal synthesis, lithography and epitaxial growth. Moreover, the properties of the QD can be altered by changing the temperature, pressure, applying magnetic or/ and electric fields. Because of this wide-broad possibility to change and design the properties of QD, they became a rich field for researchers to control their physical properties. QD open a new avenue in many technological applications such as: (QD LASER), memories, Single Electron Transistors (SET's), solar cells, quantum computers and recently spintronics.

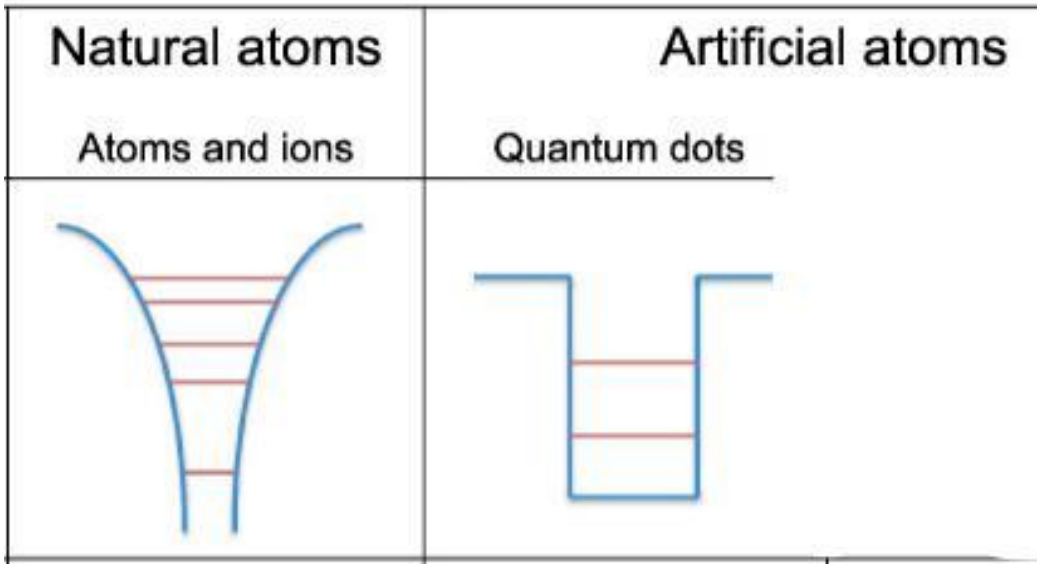

Figure 1.2: Energy levels for natural atoms and ions (at the left), and energy levels for QD [55]

In early 1980's, the first QD were successfully made in laboratories. This initiates the investigation of the properties of this heterostructure, and how they are affected and changed under certain conditions.

1.3 Heterostructure and confinement potential

In our research, the QD is made from Gallium Arsenide (GaAs) surrounded by Aluminum Gallium Arsenide(AlGaAs) semiconductor heterostructure [44].

GaAs is composed of gallium (Ga) and arsenic (As) which has a low direct bandgap, where AlGaAs is obtained by substituting some of Ga ions by Al ions which have the same number of valence electrons, with a higher band gap energy than GaAs. When Silicon (Si) is doped into the AlGaAs layer, they take place of some of As atoms, and since Si has four valence electrons while As has three; each silicon atom will release an electron as a free electron in the heterostructure. Those free electrons will move from AlGaAs layer (leaving holes) to the lower band gap of GaAs layer, where they will be trapped in the GaAs region. In this way, electrons will be free to move in the XY- plane, but its motion is quantized in the growth direction (Z- direction), it is then called 2D structure. In order to reduce the confinement, a negative voltage is applied using metal electrodes at the surface of the heterostructure, (Figure 1.3).

The lateral confinement potential is taken to be parabolic, since this model is the best to describe this confinement in postulates of quantum mechanics.

Figure (1.4) shows the confinement potential which is used to confine electrons in a QD. To demonstrate our QD Heterostructure, imagine an

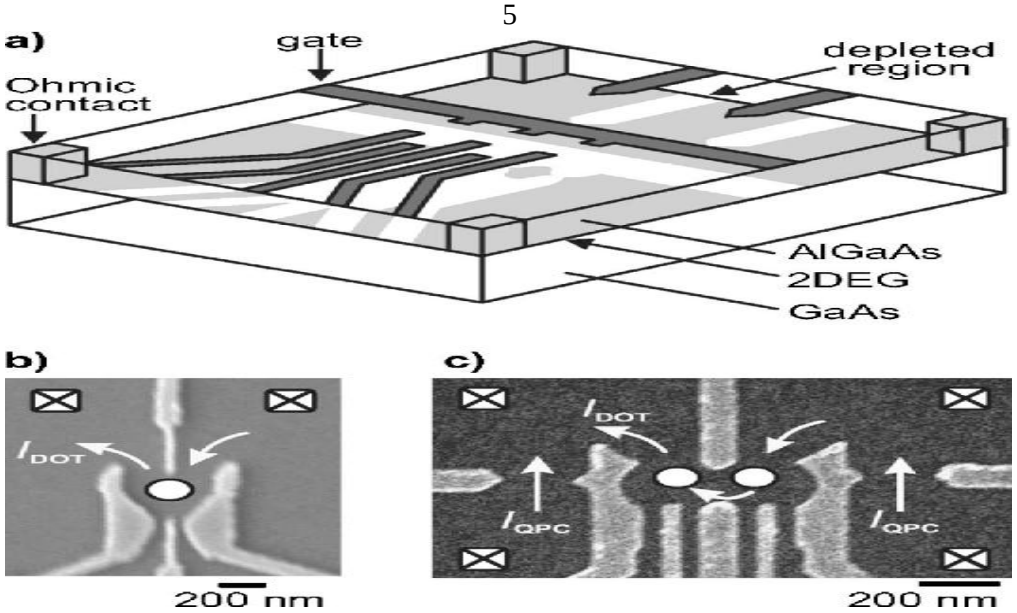

Figure 1.3: Schematic representation of GaAs/AlGaAs [56].

electron in the XY- plane, at distance r from the origin, and an impurity located at distance d on the Z axis, with applying a uniform magnetic field directed at Z direction, in addition to a tilted electric field with angels θ and ϕ as illustrated in Figure (1.5) with the presence of lateral confinement frequency ω_0.

The study of hydrogenic impurity in a QD is an important research issue in low-dimensional semiconductor systems; because the presence of impurity in nanostructure has a great influence on the electrons mobility, electronic, magnetic and optical properties [4].

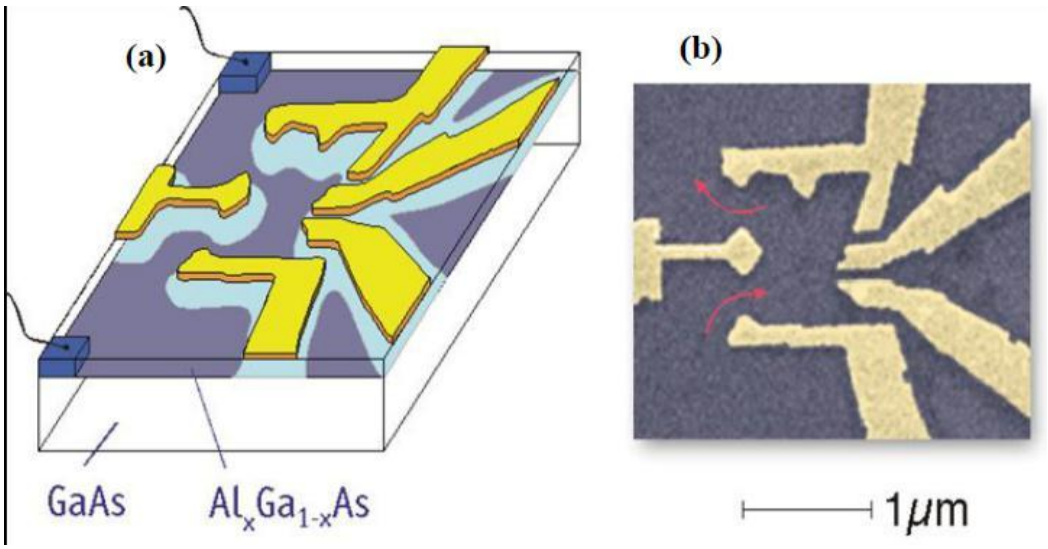

Figure 1.4: Confinement potential for QD [57]

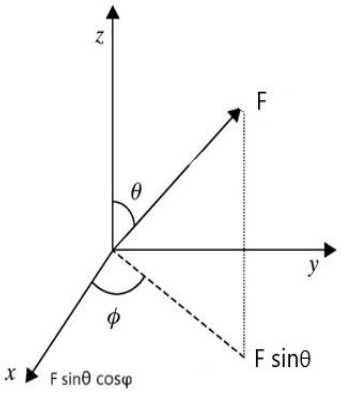

Figure 1.5: Tilted electric field.

Moreover, Rashba Spin Orbit Interaction(RSOI) has a noticeable effect on the energy Eigen values of QD, and that is a main crucial part in the very recent emerging field called Spintronics, (Figure1.6) [5].

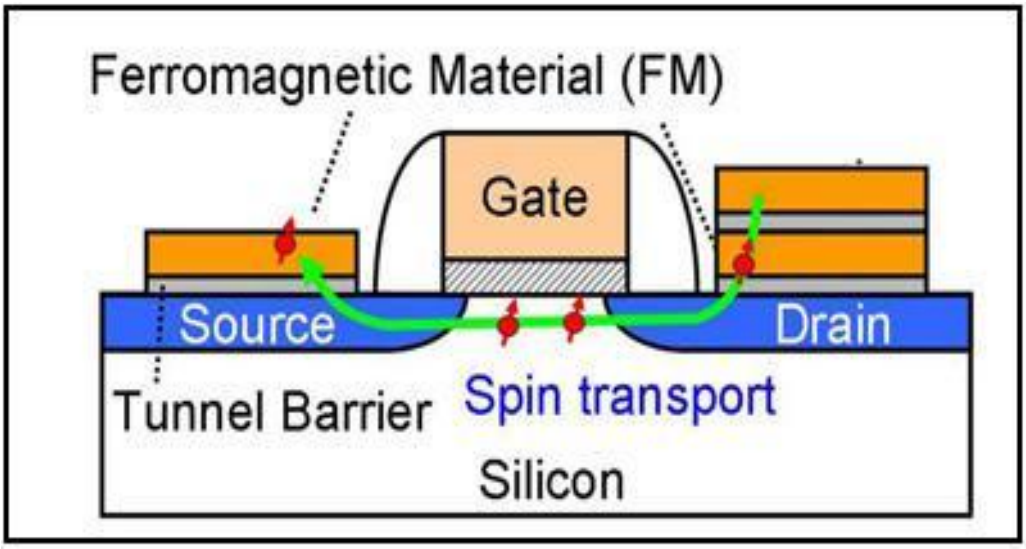

Figure 1.6: Rashba Spin Orbit interaction in Spintronics [58]**.**

1.4 Literature Review

The effect of hydrogenic impurity in QD energy spectra has been stud- ied extensively many by researchers [6–14]. Most of the work examines shallow donor in spherical QD using numerical Finite Element Method (FEM) [15] or effective mass and variational techniques [16]. The presence of hydrogenic impurity in QD affects significantly spectral properties and the energy spectra. Addition of external parameters like: magnetic [17–20], electric fields [21–23], changing the pressure and temperature [24–28], the confinement potential [29, 30], and finally Spin-Orbit Interaction [31–33] can change the electronic, magnetic and thermal properties of the QD.

Different theoretical methods had been used to solve the Hamiltonian of QD in the presence of the previously mentioned parameters. Most of the work examine shallow donor in spherical QD using numerical Finite

Ele-ment Method(FEM) [34, 35] or effective mass and variational techniques.

H. Bahramiyan et al. used variational method to study the effects of hydrostatic pressure, temperature and impurity position on the donor binding energy of a pyramid QD [4]. R. Khordad et al. studied the binding energy of diamagnetic susceptibility of a zero-temperature quantum anti dot, using analytical method [36]. A. Vanitha et al. investigated the effects of magnetic field strength on donor impurity in QW using numerical calculations [37]. They have calculated the binding energy as a function of dot size for various impurity locations, different pressure and temperature. They have found that the binding energy increases when the pressure increases, and it enhances as the temperature decreases. Elsaid studied the effect of applied magnetic field on shallow donor impurity states in a parabolic QD using ($\frac{1}{N}$) expansion [38].

Zaiping Zing et al. studied the effect of the tilted electric fields on on-center donor impurity in cylindrical QD using Potential Morphing Method (PMM) [39]. A. Chafai et al. used variational method to study the impact of the strength of an external magnetic field on the binding energy of an on - center shallow donor inside a Nano dot [40].

The combined effects of hydrostatic pressure and temperature on the binding energy of hydrogenic impurity on a spherical QD in the presence of the external electric field was solved by means of the perturbation approach, using effective mass approximation [24, 41]. XIE Wen-Fang investigated the ground state properties of a two-dimensional, two electrons QD with a Gaussian confining potential under the influence of perpendicular magnetic field using numerical diagonalization [42].

Recently, the thermodynamic properties of a QD under the presence of Rashba spin orbit interaction and magnetic field have been studied by Sukirti Gumber et al. using perturbation method [43]. G. Rezaei et al. studied the simultaneous effects of external electric field and magnetic field, hydrostatic pressure and temperature on the binding energy of a hydrostatic donor impurity in a QD using numerical integration method [44]. F. Bzour et al. calculated the energy levels of GaAs parabolic QD under the combined effects of external pressure, temperature and magnetic field using exact diagonalization method [45].

The magnetization (M) and magnetic susceptibility (χ) of a two-electrons parabolic QD in the presence of electron- electron and spin orbit interaction, had been studied by D. Sanjeev Kumar et al. [46]. M. M. Al Shorman et al. have examined the effect of magnetic field in addition to

electron-electron interaction in the thermodynamic properties of parabolic GaAs QD [47].

In this research, we have studied the effects of the presence of uniform magnetic, tilted electric fields and RSOI on the energy spectra and thermodynamic properties of a QD with a hydrogenic impurity. All the energy matrix elements are obtained in a closed analytical form. The exact diagonalization method is then implemented to diagonalize the matrix Hamiltonian and compute the QD energy spectra.

Our results are explicitly shown in chapter 3.

1.5 Research objectives

In this study, we have four main objectives, which can be summarized as follows:

1. Using exact diagonalization method to solve the Hamiltonian of donor impurity in a 2-D QD in the presence of uniform magnetic field (B with cyclotron frequency (ω_c)) and tilted electric field (F , θ), in addition to temperature (T), confining frequency (ω_0), RSOI term (α). Then, the complete energy spectra will be calculated as a function of the QD physical parameters (ω_c, F , θ, T, ω_0 and α).

2. Studying the dependency of QD magnetization on those physical parameters.

3. The computed magnetization values will be used to calculate the magnetic susceptibility as a function of QD parameters (ω_c, F, θ, T, ω_0, and α).

4. Finally, our results for the energy spectra will be used to demonstrate the behavior of QD's heat capacity under the presence of electric field, and the effect of RSOI.

1.6 Organization of the Thesis

The remainder of this thesis is organized as follows:

Chapter 2: Theory: It displays the theoretical work we followed in our computation.

Chapter 3: Results and Discussion: It displays our results and explains them.

Chapter 4: Conclusion: It summarizes the conclusions of thesis, and also suggests some possible future work.

Chapter Two
Theory

This chapter consists of three main parts that includes the details of our calculations in order to reveal the theoretical concepts we followed in our work. The main parts are:

1. QD Hamiltonian in presence of electric field, magnetic field, impurity in addition to (RSOI) term.

2. Exact diagonalization method.

3. The Magnetization, susceptibility and heat capacity of the QD.

2.1 QD Hamiltonian

The Hamiltonian of a QD in 2-D, is given by:

$$\widehat{H} = \frac{1}{2m^*} P^2 + V(r) \qquad (2.1)$$

Where:

V (r) is the confinement potential, and m^* is the effective mass of the electron, and in our work, we considered the parabolic confinement where:

$$V = \frac{1}{2}\, m^*\, \omega_0^2\, r^2 \qquad (2.2)$$

Where:

ω_0 is the confinement frequency.

and $\vec{P}$ is the kinetic momentum given by:

$$\vec{P}=-\frac{\hbar}{i}\vec{\nabla} \tag{2.3}$$

Where:

$\hbar$ is the reduced planks constant.

In our study we have considered several parameters that affect significantly the Hamiltonian of the QD. Those parameters are:

1. Magnetic Field: its effect is included in the vector potential $\vec{A}$, where:

$$\vec{A}=\frac{1}{2}\vec{\boldsymbol{B}}\times\vec{r} \tag{2.4}$$

Where $\vec{B}$ is the strength of the magnetic field, r is the radial position of the electron.

2. Presence of impurity, its effect appears as the new term in the Hamiltonian ($-\frac{e^2}{\epsilon r}$), where e is the elementary charge of the electron, and ϵ is the dielectric constant of the material (the dependence of m^* and ϵ on temperature and pressure is illustrated in appendix A In addition to the effective Rydberg units (R^*).

3. Tilted electric field (Figure 1.5), its effect appears as a new term in the Hamiltonian given by: e **F.r** = -eFr sinθ cosφ . where F is the strength of the electric field, θ and φ are illustrated in Figure 1.5. Where r and φ are the two- dimensions in polar coordinate system, while θ is a tunable parameter that F makes with Z -direction.

4. Rashba Spin-Orbit Interaction(RSOI) term, it is represented as V_R, where:

$$V_R = \sigma_z \, \alpha \, \frac{dV}{dr} \left[-i \, \frac{1}{r} \, \frac{d}{d\phi} + \frac{e \, B \, r}{2\hbar} \right] \tag{2.5}$$

V is the confinement potential, σ_z is the Pauli matrix, α is the coupling factor.

So, the total 2D-QD Hamiltonian in (r,φ) polar coordinates is given by[31, 44]:

$$\widehat{H} = -\frac{1}{2m^*} \left(\vec{P} + \frac{e}{c} \vec{A} \right)^2 - \frac{e^2}{\epsilon r} + e \, \vec{F} \, . \vec{r} + \frac{1}{2} \, m^* \omega_0^2 \, r^2 +$$

$$\sigma_z \, \alpha \, \frac{dV}{dr} \left[-i \, \frac{1}{r} \, \frac{d}{d\phi} + \frac{e \, B \, r}{2\hbar} \right] \tag{2.6}$$

where: c is the speed of light.

The Hamiltonian using the symmetric gauge for A; where A=B (-y, x,0), can be expressed as:

$$H = -\frac{\hbar^2}{2m^*} \nabla^2 r + \frac{1}{2} \, m^* \, \omega_0^2 \, r^2 + \frac{1}{8} \, m^* \, \omega_c^2 \, r^2 - \frac{e^2}{\epsilon r} + eFr \, sin\theta \, cos\phi$$
$$+ \frac{1}{2} \, \hbar \omega_c L_z + \left[\frac{2s\alpha m^* \, \omega_c \omega_o^2}{\hbar} \right] L_z + \left[\frac{2s\alpha m^* \, \omega_c \omega_o^2}{\hbar} \right] r^2 \tag{2.7}$$

Where s is the spin of the electron, and L_z is the angular momentum.

which can be rewritten as:

$$H = -\frac{\hbar^2}{2m^*} \nabla^2 r + \frac{1}{2} \, m^* \, r^2 \left[\frac{1}{2} \, \omega_c^2 + \omega_0^2 \left[1 + \frac{2s\alpha m^* \, \omega_c \omega_o^2}{\hbar} \right] \right] - \frac{e^2}{\epsilon r} +$$
$$eFr \, sin\theta \, cos\phi + \left[\frac{1}{2} \, \hbar \omega_c + \frac{2s\alpha m^* \, \omega_c \omega_o^2}{\hbar} \right] L_z \tag{2.8}$$

and can be represented as:

$$H = H_0 + H_1 \tag{2.9}$$

where:

$$H_0 = -\frac{\hbar^2}{2m^*}\nabla^2 r + \frac{1}{2}m^* r^2\left[\frac{1}{2}\omega_c^2 + \omega_0^2\left[1 + \frac{2s\alpha m^*\omega_c\omega_o^2}{\hbar}\right]\right] \tag{2.10}$$

And,

$$H_1 = -\frac{e^2}{\epsilon r} + eFr\,sin\theta\,cos\phi + \left[\frac{1}{2}\hbar\omega_c + \frac{2s\alpha m^*\omega_c\omega_o^2}{\hbar}\right]L_z \tag{2.11}$$

where: ω_0 is the confinement frequency, and ω_c is cyclotron frequency given by:

$$\omega_c = \frac{eB}{m^* c} \tag{2.12}$$

H_0 is a harmonic oscillator type Hamiltonian with effective frequency ω_{eff}.

$$\omega_{eff} = \frac{1}{4}\omega_c^2 + \omega_0^2\left[\frac{2s\alpha m^*\omega_c}{\hbar}\right] \tag{2.13}$$

with well-known Eigen functions Ψ_{nm} and eigenenergy spectra E_{nm}, Fock-Darwin states [48, 49], are given as:

$$\Psi_{nm} = N_{nm}\frac{e^{im\phi}}{\sqrt{2\pi}}(\beta r)^{|m|}e^{-\frac{\beta^2 r^2}{2}}L_n^{|m|}(\beta^2 r^2) \tag{2.14}$$

And,

$$E_{nm} = (2n + |m| + 1)\hbar\omega_{eff} \tag{2.15}$$

where:

n: is the radial quantum number, n=0,1,2,3, 4, ….

m: is the magnetic quantum number, m=0, ±1, ±2, ±3, ±4, …

$L_n^{|m|}$: is the associated Laguerre polynomials.

N: is the normalization constant given by:

$$N = \sqrt{\frac{2n!\,\beta^2}{(2n+|m|)!}} \tag{2.16}$$

and,

$$\beta = \sqrt{\frac{m^2\,\omega_{eff}}{h}} \tag{2.17}$$

The existence of the second part in the Hamiltonian in equation 2.9, makes the analytical solution unobtainable. So, we will apply Exact Diagonalization Method (EDM) as a powerful technique to solve the above Hamiltonian.

2.2 Exact Diagonalization Method

To obtain the energy spectra for the total Hamiltonian given in equation 2.9 we have used EDM (see Appendix B), we need to construct a matrix Hamiltonian as:

$$H_{nm,n'm'} = \langle \Psi_{nm} | H | \Psi_{,n'm'} \rangle \tag{2.18}$$

Then, diagonalize that matrix ($H_{nm,n'm'}$) and extract the lowest eigenvalue using Mathematica package. A very important step was to

write ($H_{nm,n'm'}$)in the simplest closed form to reduce the execution time needed for the diagonalization process.

The matrix terms of the Hamiltonian in equations 2.10 and 2.11 (using effective Rydberg units in our program) are obtained in a closed analytical form as given below:

$$1.\langle\Psi_{nm}|H_0|\Psi_{,n'm'}\rangle = (2n + |m| + 1)\omega_{eff}\,\delta_{nn'}\delta_{mm'} \tag{2.19}$$

$$2.\left\langle\Psi_{nm}\left|\left[\frac{1}{2}\,\hbar\omega_c + \frac{2s\alpha m^*\omega_o^2}{\hbar}\right]L_z\right|\Psi_{,n'm'}\right\rangle = \left(\frac{1}{2}\,m\,\omega_c m\,s\,\alpha\,\omega_0^2\right)\delta_{nn'}\delta_{mm'} \tag{2.20}$$

$$1.\left\langle\Psi_{nm}\left|-\frac{e^2}{\epsilon r}\right|\Psi_{n'm'}\right\rangle = -\frac{2}{\epsilon}\int_0^\infty\int_0^{2\pi}\Psi_{nm}\frac{1}{r}\,\Psi_{n'm'}\,r\,dr\,d\phi \tag{2.21}$$

To evaluate the radial part of the integral, we used the property of Laguerre's polynomial relation [50]:

$$\int_0^\infty y^{\mu-1}\,e^{-\kappa y}\,L_m^\tau(ay)L_n^\eta(by)dy = \frac{\Gamma(\mu)(\tau+1)_m(\eta+1)_n}{m!n!}\,\kappa^{-\mu}\sum_{j=1}^m\frac{(-m)_j(\mu)_j}{(\tau+1)_j j!}\left(\frac{a}{\kappa}\right)^j\sum_{\kappa=1}^n\frac{(-n)_j(\mu+j)_\kappa}{(\tau+1)_\kappa\kappa!}\left(\frac{b}{\kappa}\right)^\kappa \tag{2.22}$$

So, the coulomb matrix term in equation 2.21 reads as,

$$\left\langle\Psi_{nm}\left|-\frac{e^2}{\epsilon r}\right|\Psi_{n'm'}\right\rangle = \frac{2}{\epsilon}\frac{\Gamma\left(m+\frac{1}{2}\right)(m+1)_n(m+1)_{n'}}{n!n'!}\sum_{j=1}^n\frac{(-n)_j(m+\frac{1}{2})_j}{(m+1)_j j!}\sum_{\kappa=1}^{n'}\frac{(-n')_\kappa(m+j+\frac{1}{2})_\kappa}{(m+1)_\kappa\kappa!} \tag{2.23}$$

4. The electric field energy contribution is:

$$\langle\Psi_{nm}|eFr\,sin\theta cos\phi|\Psi_{,n'm'}\rangle = \sqrt{2}\,F\,sin\theta\int_0^\infty\int_0^{2\pi}\Psi_{nm}\,\Psi_{n'm'}\,r^{\,2}dr\,cos\phi d\phi \tag{2.24}$$

To simplify equation (2.24) , we have followed the same steps as before, but here the integration over φ is not (2π) anymore, because of the existence of (cosφ) and the integration is evaluated by rewriting (cosφ = $\frac{e^{i\phi}+e^{-i\phi}}{2}$).

So, when applying the relation in equation 2.22 we had two terms, the first term with $\frac{e^{i\phi}}{2}$ multiplied by $\Psi_{n'm'}$, and this shift m' to m'+1, so, a new selection rule will appear as ($\delta_{m',m'+1}$). And the other term $\frac{e^{-i\phi}}{2}$ is multiplied by $\Psi_{n'm'}$, and this shift m' to m'-1, and so, another selection rule appears ($\delta_{m',m'-1}$).

$$\langle\Psi_{nm}|eFr\ sin\theta cos\phi|\Psi_{n'm'}\rangle = \frac{\sqrt{2}F\ sin\theta}{4}\left(\frac{\Gamma(m+1)(m+1)_n(m+1)_{n'}}{n!n'!}\sum_{j=1}^{n}\frac{(-n)_j(m+1)_j}{(m+1)_j j!}\sum_{\kappa=1}^{n'}\frac{(-n')_\kappa(m+j+1)_\kappa}{(m-1)_\kappa\kappa!}+\frac{\Gamma(m+2)(m+1)_n(m+1)_{n'}}{n!n'!}\sum_{j=1}^{n}\frac{(-n)_j(m+2)_j}{(m+1)_j j!}\sum_{\kappa=1}^{n'}\frac{(-n')_\kappa(m+j+2)_\kappa}{(m+2)_\kappa\kappa!}\right) \quad (2.25)$$

and now, after all that work, our $H_{nn'}$ is ready, and we extracted our results for the energy eigenvalues, and used them to investigate the dependence of both magnetic (M and χ) and thermodynamic (C_v) properties of our QD on several parameters (B, F, θ and ω_0, T and α).

2.3 Magnetization of the QD

The Magnetization is a description of how magnetic materials react to a magnetic field. and it can be calculated by taking the magnetic field first derivative of the mean energy of the QD [51]:

$$M = -\frac{\partial\langle E(B,F,\theta,\omega_0,T,\alpha\rangle}{\partial B} \quad (2.26)$$

where, $\langle E\ (B, F, \theta, \omega_0, T, \alpha)\ \rangle$ is the statistical energy of the QD given by:

$$\langle E(B, F, \theta, \omega 0, T, \alpha)\rangle = \frac{\sum_{j=1}^{N} E_j\, e^{-\frac{E_j}{K_B T}}}{\sum_{j=1}^{N} e^{-\frac{E_j}{K_B T}}} \tag{2.27}$$

The summation is taken over the energy spectrum of the QD.

2.4 Susceptibility of the QD

Magnetic Susceptibility indicates whether the material will be attracted to (+ χ ' paramagnetic') or repelled out of (- χ 'diamagnetic') a magnetic field. χ is calculated from M by [46]:

$$\chi = \frac{\partial \langle E(B,F,\theta,\omega_0,T,\alpha\rangle}{\partial M} \tag{2.28}$$

2.5 Heat Capacity

Heat capacity of a material is the amount of heat needed to raise that material's temperature by one degree, and it can be calculated for QD by [52]:

$$C_v = \frac{\partial \langle E(B,F,\theta,\omega_0,T,\alpha\rangle}{\partial T} \tag{2.29}$$

Chapter 3
Results and Discussion

In this chapter we will present our computed results for the effects of applied fields and the Rashba Spin-Orbit Interaction coupling on the energy levels, magnetic and thermodynamic properties of the QD.

This chapter is organized as follows:

1. Convergency.

2. Binding energy

3. Statistical energy

4. Magnetization and Susceptibility

5. Heat Capacity

The physical parameters for GaAs - QD material used in our work (at zero Kelvin, and zero pressure).

1. Effective Rydberg (R*) = 5.694 meV

2. Dielectric constant (ϵ) =12.655 ϵ_0, where ϵ_0 is the dielectric permittivity of free space.

3. Effective mass of electron = 0.0669 $m_{0,}$ where m_o is the mass of free electron.

3.1 Convergency

The first step in our work is to ensure the convergency issue, to guarantee that our desired energy spectra are accurate. In our calculations, we have changed the number of basis, until we have obtained the convergent energy values as shown in tables 3.1, 3.2, and 3.3.

Our chosen basis was 72x72 (the angular quantum number m was taken to be (- 4 → 4) and the radial quantum number n (0 → 7)) where there was a stability in the values of the ground state energy as shown in Figure 3.1.

TABLE 3.1: The values of the Ground state energy and the basis of the matrix, with changing angular quantum number m from -4 → 4 and the radial quantum number n is taken from 0 → 5 at ω_0=3R*,ω_c=2R*, F=5 R*, $\hbar = 1$ ($Rydberg\ units$).

No. of basis	Ground state energy (meV)
0	-14.9319
18	-19.7069
30	-20.1743
42	-20.2128
54	-20.2154
66	-20.2155
78	-20.2155
90	-20.2155

TABLE 3.2: The values of the Ground state energy and the basis of the matrix, with changing angular quantum number m from -4 → 4 and the radial quantum number n is taken from 0 → 7, at ω_0=3R*, ω_c=2R*, F=5 R*, $\hbar = 1$ ($Rydberg\ units$).

No. of basis	Ground state energy meV
0	-15.65
24	-20.2647
40	-20.7079
56	-20.7438
72	-20.7461
88	-20.7463
104	-20.7463
120	-20.7463

After the convergency issue is fulfilled, the next step is to calculate the Binding energy.

TABLE 3.3: The values of the Ground state energy and the basis of the matrix, with changing angular quantum number m from -4 → 4 and the radial quantum number n is taken from 0 → 7, at ω_0=2R*, ω_c=2R*, F=5 R*, $\hbar = 1$ ($Rydberg\ units$).

No. of basis	Ground state energy (meV)
0	-16.9567
24	-24.1065
40	-25.6193
56	-25.9671
63	-26.0399
72	-26.0522
88	-26.076
104	-26.0831
120	-26.0852
136	-26.0854
152	-26.0858
168	-26.0859
184	-26.0859

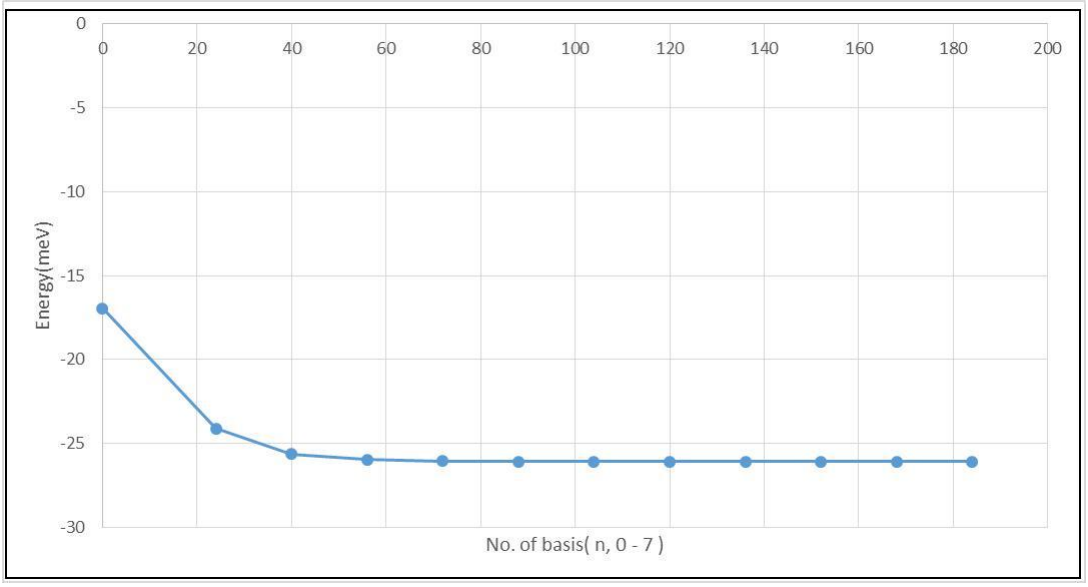

Figure 3.1: Ground state Energy Vs No. of basis, with F= 4.8 R*, ω_0= 2 R*, ω_c = 2R*, T = 0.01 K, θ = 60 ^{0}, $\hbar = 1$ $(Rydberg\ units)$.

3.2 Binding Energy

In this section we present our computed results for binding energies of the donor impurity under several QD physical parameters.

In Figure (3.2), we have plotted Binding energy against ω_c for different values of ω_0, the figure shows that the binding energy increases as ω_c increases. This is expected behavior; due to the presence of a magnetic field

which adds new confinement for the electron as can be seen from equation

(2.13). In Figure (3.2), we have shown the dependence of the donor binding energy in the QD, on the magnetic field for various confinements, ω_0 = 4R*, 6R*, and 8R*, comparing the three plotted lines: when the confine-ment frequency increases, that means more binding of the donor

impurity (higher binding energy), and that appears clearly in the Figure (3.2).

In addition, in Figure (3.3) we have examined the effect of electric field on the binding energy for different values of ω_0. As shown in the figure; the binding energy decreases, as the electric field increases, and this is because the electric field tends to separate the electron, i.e. it moves the electron away, increasing the distance between the electron and the nucleus decreasing the confinement and the Coulomb interaction, and hence decreasing the binding energy, the numerical results are presented in table (3.4).

Figure (3.5) shows the change in binding energy due to the change of the tilted angle of the electric field. In that figure, as θ increases, the component of electric field increases, having the same effect on the binding energy as increasing F, and the figure shows the dependence of the binding energy on the electric field.

All the results shown in the figures mentioned above are with good qualitative agreement of the results of reported works in [23, 44].

Finally, to present the effect of RSOI; we have plotted the binding energy against ω_0 in the presence of RSOI in Figure (3.4) and table (3.5). As shown in the figure, the effect of RSOI appears at higher ω_0, where the coupling decreases the binding energy.

The presence of spin down (-s) RSOI decreases the binding energy, and that because the negative sign that comes from the spin down decreases the effective frequency as shown in equation (2.13).

TABLE 3.4: The binding energy for different values of electric field (F) and ω_0, ω_c= 2R*, T= .01 K, θ = 60 ^{0}, $\hbar = 1$ ($Rydberg\ units$).

F(R*)	Binding energy meV (ω_0 = 6R*)	Binding energy meV (ω_0 =8R*)
0	43.058	47.814
4	41.522	46.991
8	37.554	44.716
12	32.257	41.416
16	26.462	37.513
20	20.848	33.327
24	16.085	29.1
28	12.599	25.035
32	10.286	21.314

TABLE 3.5: Binding energy for different values of ω_0, and with/without RSOI coupling, with F= 4 R*, ω_c= 2 R*, T=.01 K, θ = 60 ^{0}, $\hbar = 1$ ($Rydberg\ units$).

ω_0 (R*)	binding energy meV(α=0)	binding energy meV (α= 20 meV.nm)
0	1.747	1.747
1.5	5.457	5.431
2	12.635	10.814
3.5	19.274	16.613
3	24.145	21.125
3.5	27.917	24.577
4	31	27.238
4.5	33.615	29.248
5	35.896	30.603
5.5	37.929	31.102
6	39.773	30.284

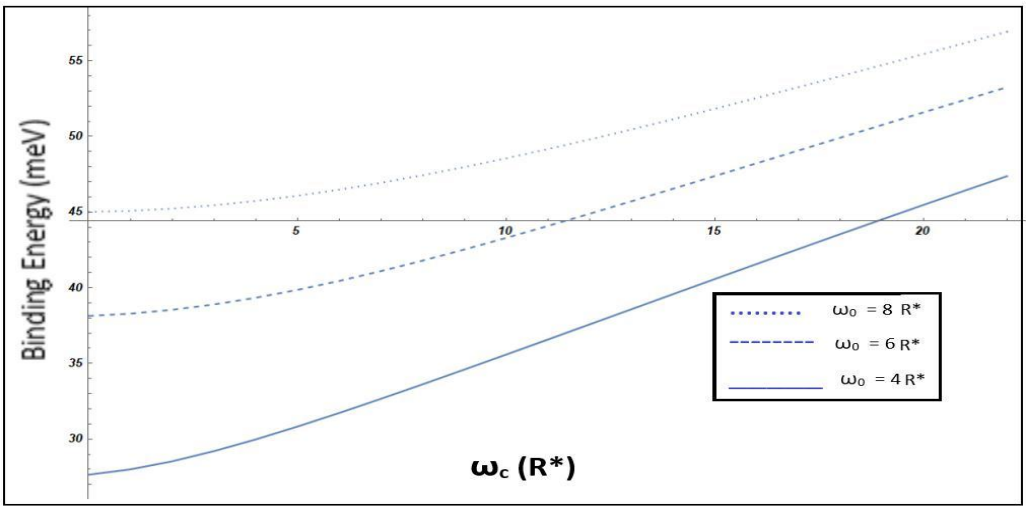

Figure 3.2: Binding Energy Vs ω_c for Different values of confinement frequency ω_0 = (8 R* for dotted line, 6R* for dashed line, 4 R* for solid line), with F= 4.8 R*, T = 0.01 K, θ = 60 ^{0}, $\hbar = 1$ $(Rydberg\ units)$.

Now, in the next two sections, our computed work for: Statistical energy, Magnetization, Susceptibility will be presented with the effect of: Electric field strength (F), Temperature(T), Confinement frequency (ω_0), Tilted angle (θ), presence of impurity, presence of RSOI and the strength of RSOI coupling, respectively.

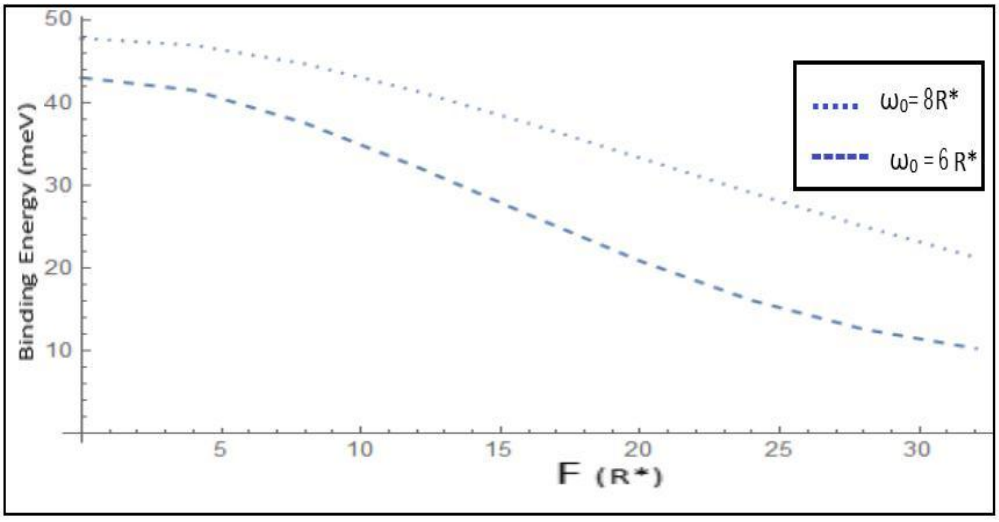

Figure 3.3: Binding Energy Vs electric field for different values of confinement frequency ω_0 = (8 R* for dotted line, 6R* for dashed line with ω_c= 2 R*, T = 0.01 K, θ = 60 ^{0}, $\hbar = 1$ $(Rydberg\ units)$

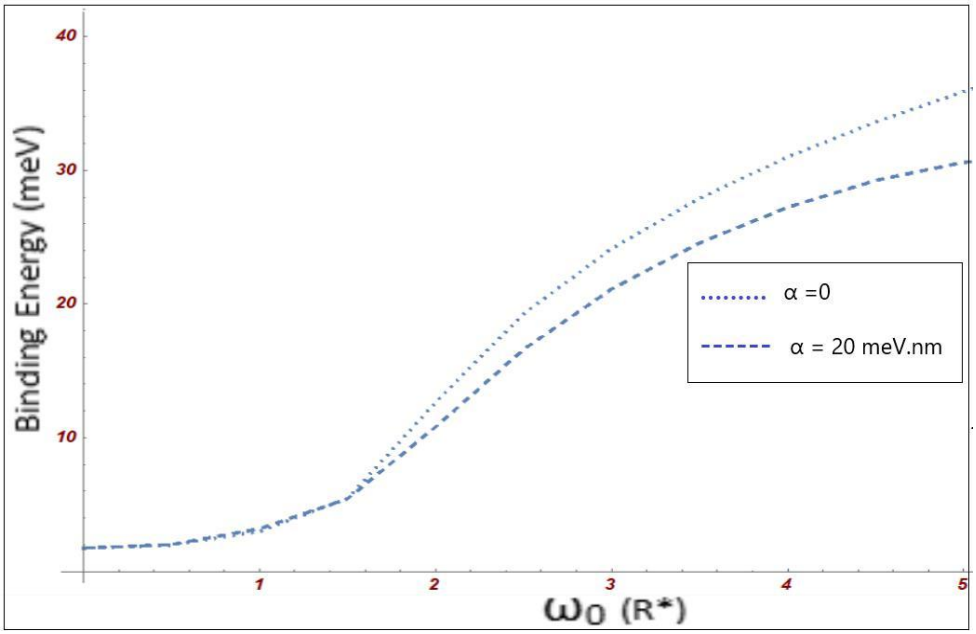

Figure 3.4: Binding Energy vs w_0 with/without RSOI coupling dashed/ dotted, for F= 4.8 R*, ω_c= 2 R*, T = 0.01 K, θ = 60 ^{0}, $\hbar = 1$ $(Rydberg\ units)$.

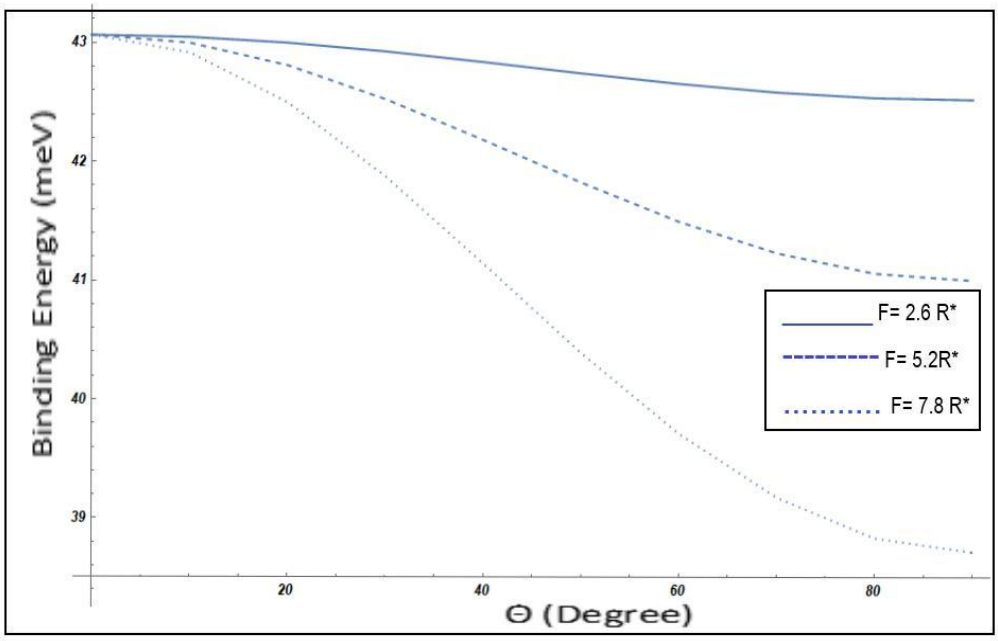

Figure 3.5: Binding Energy vs θ for different values of electric fields F = (2.6 R* for solid line, 5.2 R* for dashed line, 7.8 R* for dotted line), with ω_0=2 R*, T = 0.01 K, ω_c =2R*, $\hbar = 1$ $(Rydberg\ units)$.

3.3 Statistical Energy

In order to obtain our desired results for the magnetic properties of the QD, we first computed the statistical energy as important quantity, from which we can derive all the thermodynamic quantities. defined in equation (2.27).

The effect of electric field on the statistical energy is plotted in Figure (3.6). The figure shows that when the electric field strength gets higher, the

statistical energy gets lower, because the electric field tries to separate the electron from the donor impurity, thereby, the binding energy gets lower, and so, the statistical energy decreases.

In Figure (3.7), as the magnetic field increases, the statistical energy increases too, and that is due to the additional confinement of the electron by the magnetic field, and for different values of temperature, one can see from the figure that for higher temperature, the statistical energy is higher, and that is consistent with reference [53].

The effect of ω_0 is presented In Figure (3.8), where we can figure out that ω_c has more effect on the statistical energy when w_0 is lower, while when

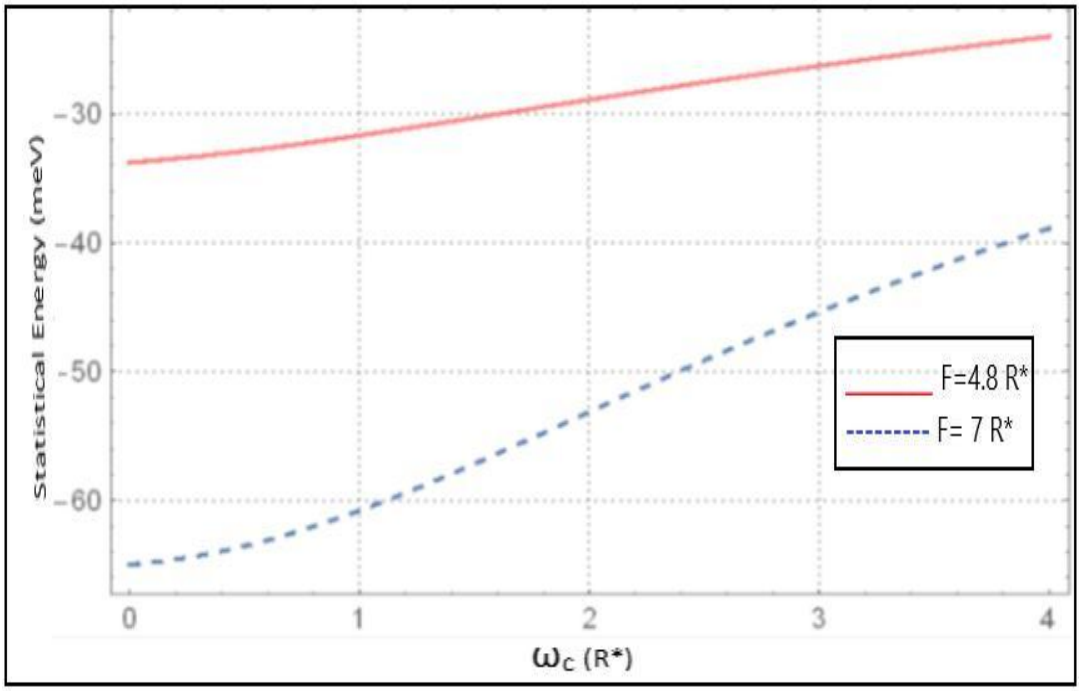

Figure 3.6: Statistical Energy against ω_c for different values of F (F= 4.8 R* for solid line, = 7 R* for dashed line), ω_0= 2 R*, T = 0.01 K, θ = 60 ^{0}, $\hbar = 1$ $(Rydberg\ units)$.

ω_0 is higher, the effect of ω_c is minor, and in general, as w_0 increases, the effective frequency ω_{eff} enhances the statistical energy.

In addition, changing the tilted angle θ affects the energy values, as presented in Figure (3.9), as the angle θ increases, the strength of the electric field term increases also, which leads to quite large separation of the electron from the donor impurity. In this case, the binding energy of the donor impurity decreases since the Coulomb attractive energy reduces, ($V_c \sim e^2/r$) also, the presence of impurity shifts the energy values to higher levels, (Figure 3.10).

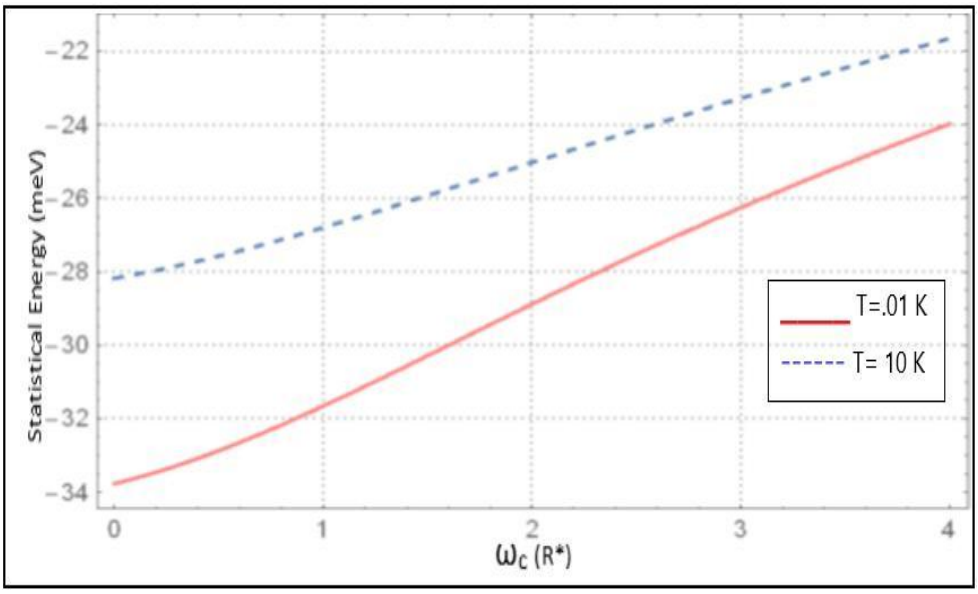

Figure 3.7: Statistical Energy against ω_c for different values of T (T= .01 K for solid line, =10 K for dashed line), ω_0= 2 R*, F = 4.8 R*, θ = 60 ^{0}, $\hbar = 1$ ($Rydberg\ units$).

The presence of RSOI and the effect of strength of coupling is presented in Figures (3.11), and (3.12), respectively. RSOI coupling lowers the statistical energy. In the strong coupling case, the statistical energy values are lower than that of weak coupling for low values of ω_c, while at higher ω_c the situation is reversed.

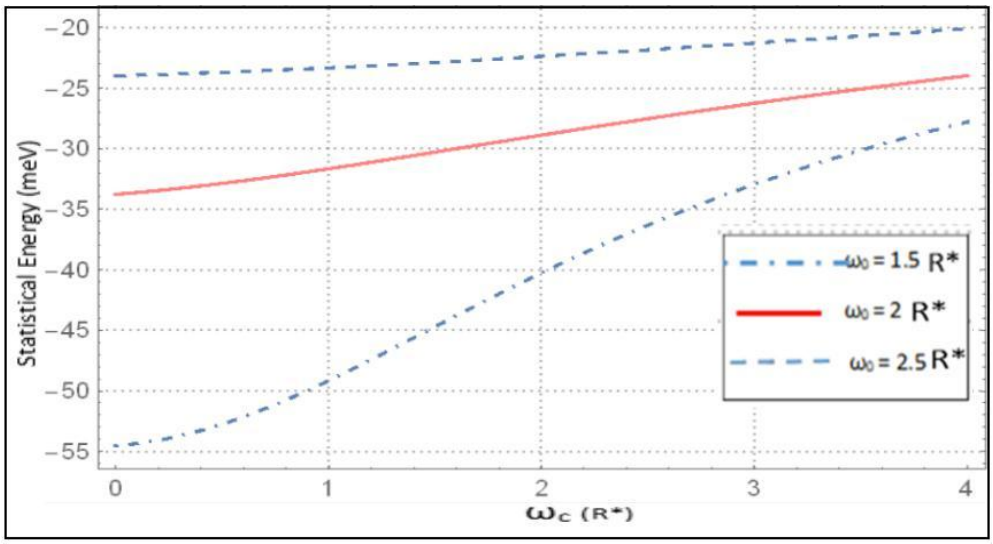

Figure 3.8: Statistical Energy against ω_c for different values of ω_0 (ω_0 = 2 R* for solid line, = 2.5 R* for dashed line, = 1.5 R* for dot dashed), T= .01 K, F = 4.8 R*, θ = 60 ^{0}, $\hbar = 1$ ($Rydberg\ units$).

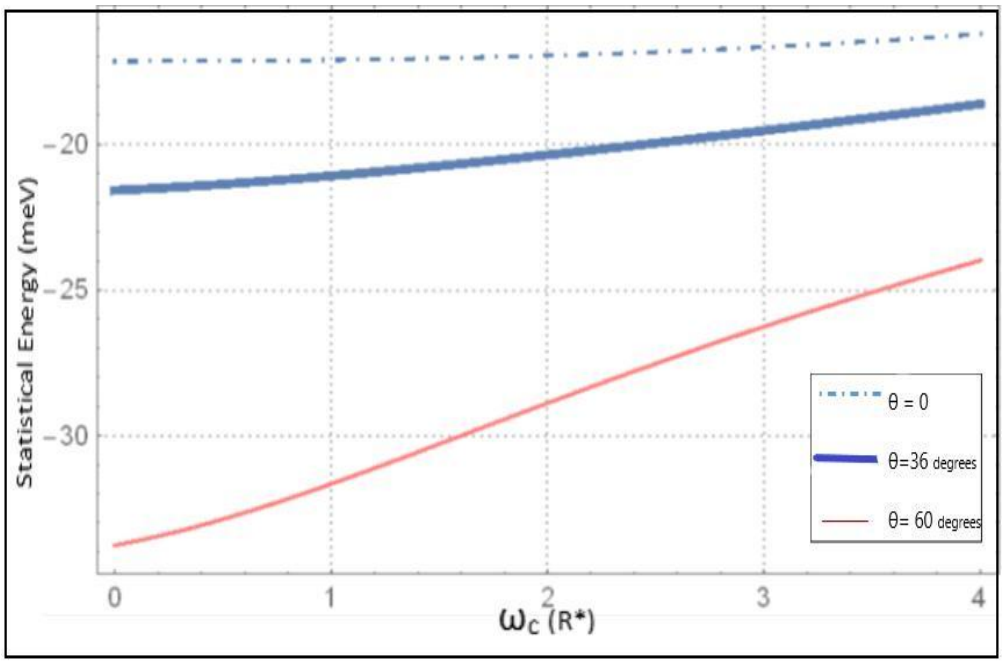

Figure 3.9: Statistical Energy against ω_c for different values of θ (θ =60 ^{0} for solid line, =36^0 for thick line, = 0 for dot dashed line), ω_0= 2 R*, F = 4.8 R*, T= .01K, $\hbar = 1$ $(Rydberg\ units)$.

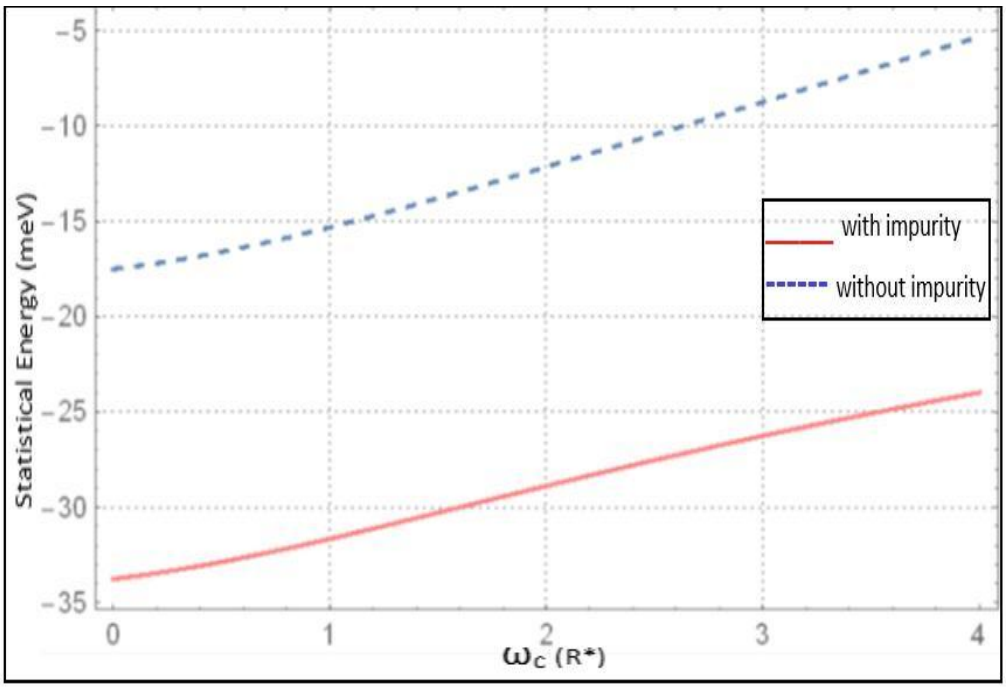

Figure 3.10: Statistical Energy against ω_c with (dashed line)/without (solid line) impurity, ω_0= 2 R*, F = 4.8 K, θ = 60 ^{0}, T= .01 K, $\hbar = 1$ $(Rydberg\ units)$.

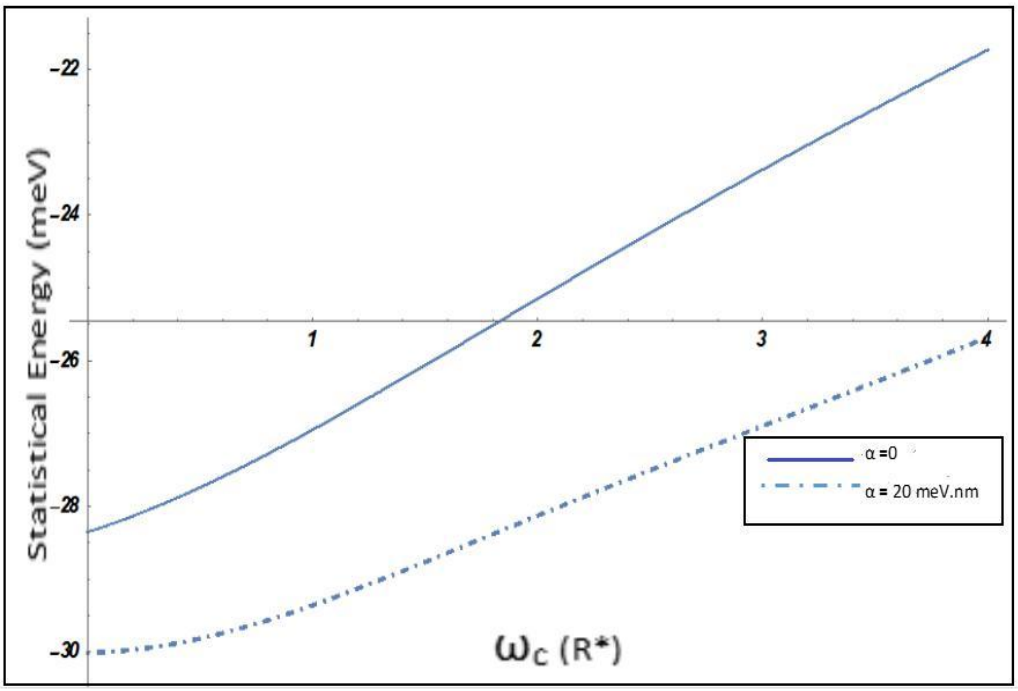

Figure 3.11: Statistical Energy against ω_c with (dot dashed line)/without (solid line) RSOI, ω_0= 2 R*, F = 4.8 K, θ = 60 ^{0}, T= .01 K, $\hbar = 1$ $(Rydberg\ units)$.

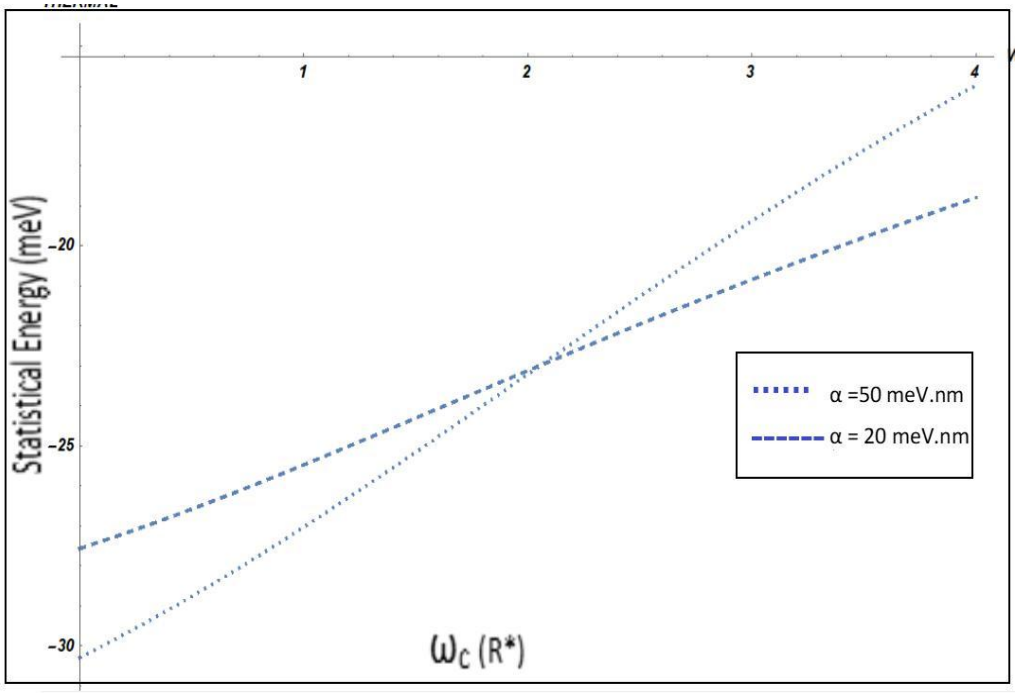

Figure 3.12: Statistical Energy against ω_c with different values of RSOI coupling (α= 50 meV.nm for dotted line, = 20 meV.nm for dashed line), ω_0= 2 R*, F = 4.8 K, θ = 60 ^{0}, T= .01 K, $\hbar = 1$ $(Rydberg\ units)$.

3.4 Magnetization and Susceptibility

In this section, our computed results for the M and χ for all the statistical energy figures presented in the previous section, are shown in the same order they appeared previously.

The variation of M as a function of $\omega_c$at various values of F is shown in Figure (3.13). In both cases for F, as $\omega_c$increases, M decreases (or |M| increases) till ω_c reaches critical value, then it starts to increase. This change means the transition from - χ (Diamagnetic material) into + χ (Paramagnetic material) as shown in Figure (3.14), this transition

took place when F is low at lower ω_c, while for high F, the peak in M occurs at higher ω_c. For fixed values of ω_c, the magnetization decreases as the electric field strength increases. This result is consistent with the donor energy be- haviour against the electric field shown previously.

The change in the behavior of M is due to the electric field effect, which leads to the flipping in the sign of χ from diamagnetic (- χ) to paramagnetic material (+ χ).

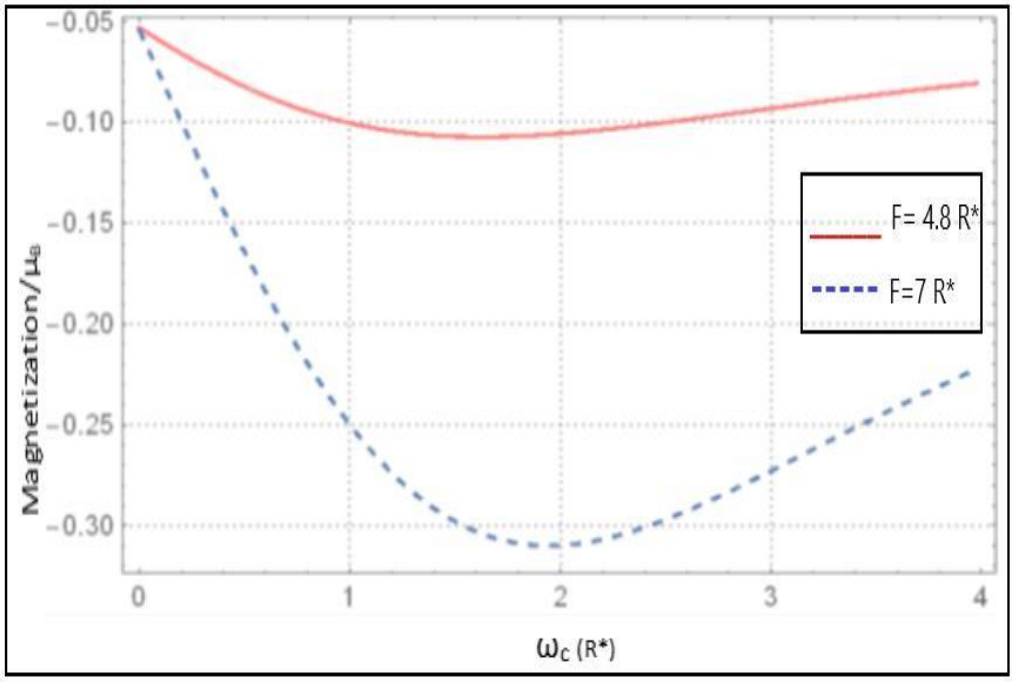

Figure 3.13: Magnetization vs ω_c with different F values (F= 4.8R* for solid line, = 7 R* for dashed line) Different values of electric fields F = (2.6 R* for solid line, 5.2 R* for dashed line, 7.8 R* for dotted line), with ω_0=2 R*, T = 0.01 K, θ =60^0 $\hbar = 1$ ($Rydberg\ units$).

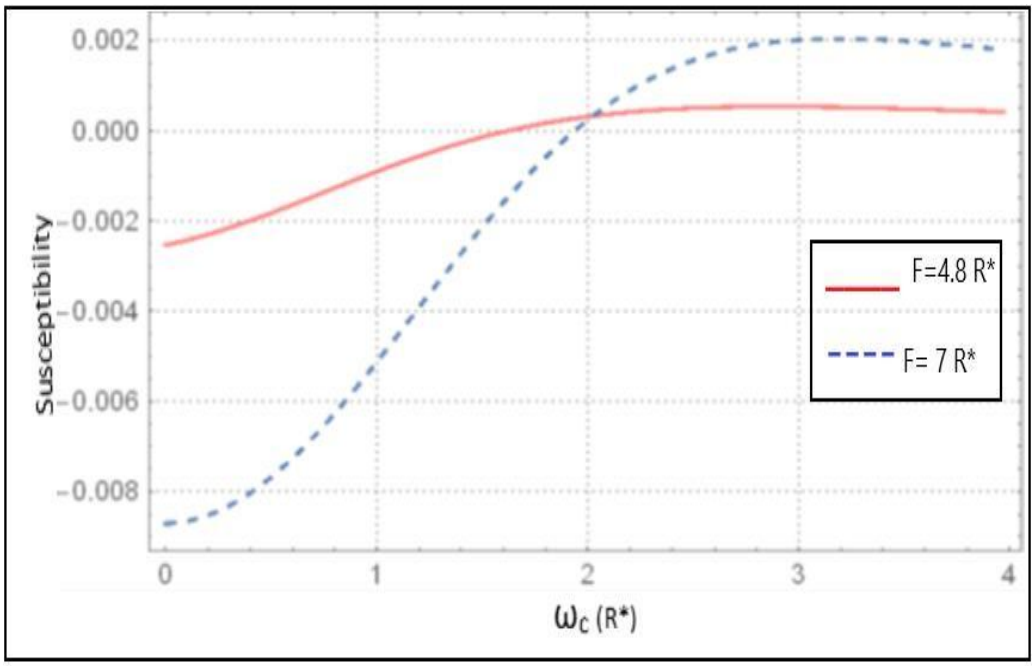

Figure 3.14: Susceptibility vs ω_c with different F values (F= 4.8R* for solid line, = 7 R* for dashed line), with w_0=2 R*, T = 0.01 K, θ =60 ^{0} $\hbar = 1$ ($Rydberg\ units$).

As a result, the electric field strength allows us to tune and control the magnetic type of the QD material.

It is quite the same behavior of M and consequently of c that appears when M and χ are plotted against ω_c as shown in Figures (3.15), and (3.16), where it is clear that for low temperature, the transition from decreasing M case (i.e. Diamagnetic region) to the increasing M case (paramagnetic region) occurs at low value of ω_c, while the effect of T appears at higher T, where the transition occurs at higher ω_c.

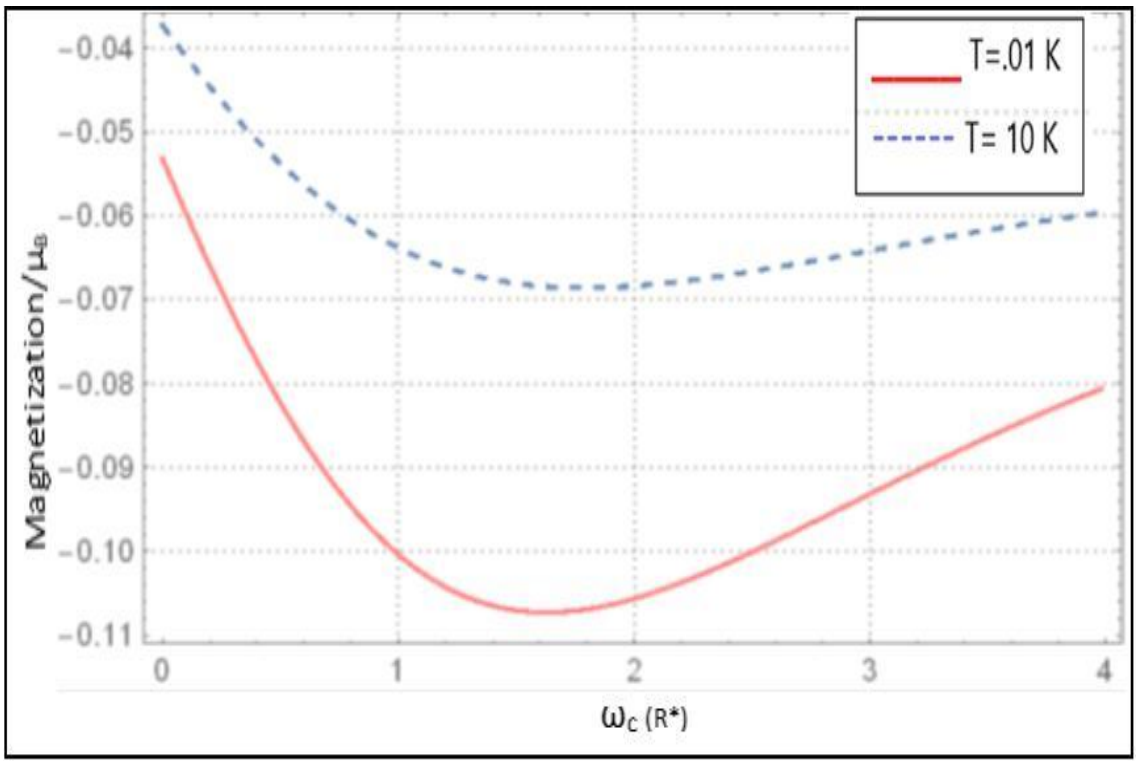

Figure 3.15: Magnetization vs ω_c with different T values (T= .01 K for solid line, = 10 K* for dashed line) with ω_0=2 R*, F =4.8 R*, θ =60 ^{0}, $\hbar = 1$ ($Rydberg\ units$).

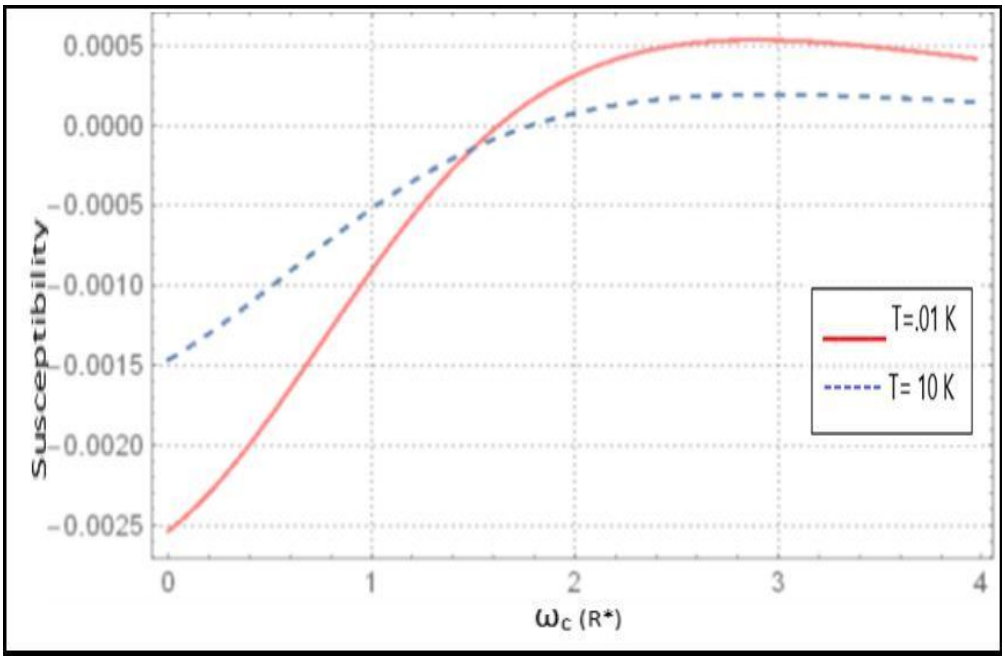

Figure 3.16: Susceptibility vs ω_c with different T values (T= .01 K for solid line, = 10 K* for dashed line) with ω_0=2 R*, F =4.8 R*, θ =60 ^{0}, $\hbar = 1$ $(Rydberg\ units)$.

At low magnetic field, the thermal energy is becoming more significant, and it enhances χ as the temperature increases. However, as the magnetic field increases, χ decreases with increasing temperature as expected.

The effects of ω_0 on M and χ are presented in Figures (3.17), and (3.18) . The transition occurs more quickly for low confinement, while at higher confinement the transition gets slower, even disappears at higher values.

For quite high magnetic field, (ω_c >> 1.5 R*), χ is higher for higher values of ω_0 , due to the large confinement of the electron in the QD.

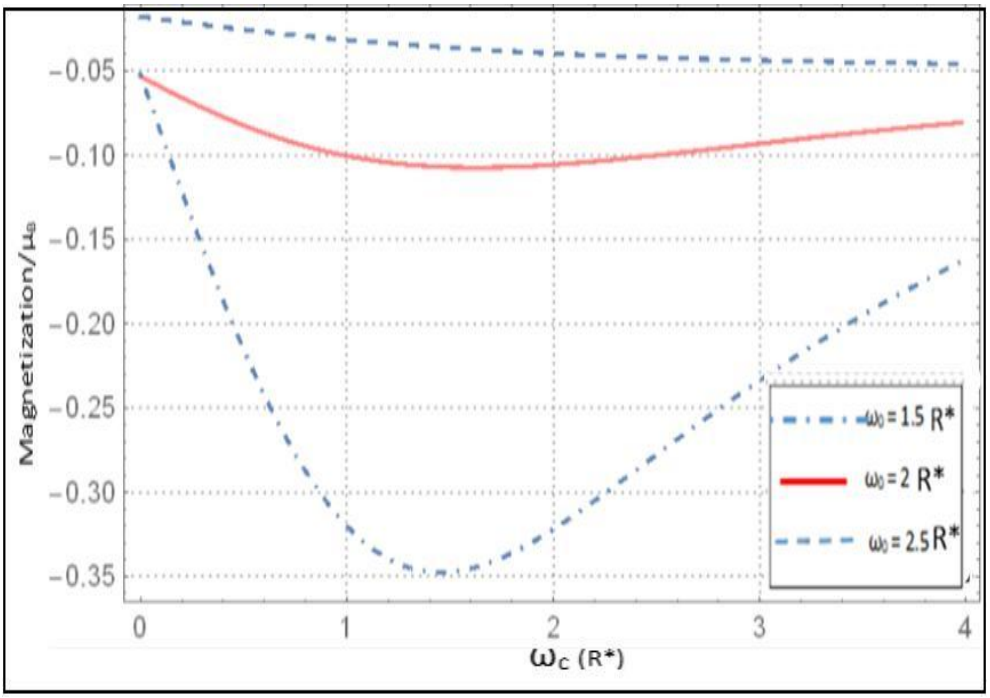

Figure 3.17: Magnetization vs ω_c with different ω_0 values (ω_0=2R* for solid line, = 2.5 R* for dashed line, = 1.5 R* for dot dashed) with T= .01 K, F =4.8 R*, θ =60 ^{0}, $\hbar = 1$ $(Rydberg\ units)$.

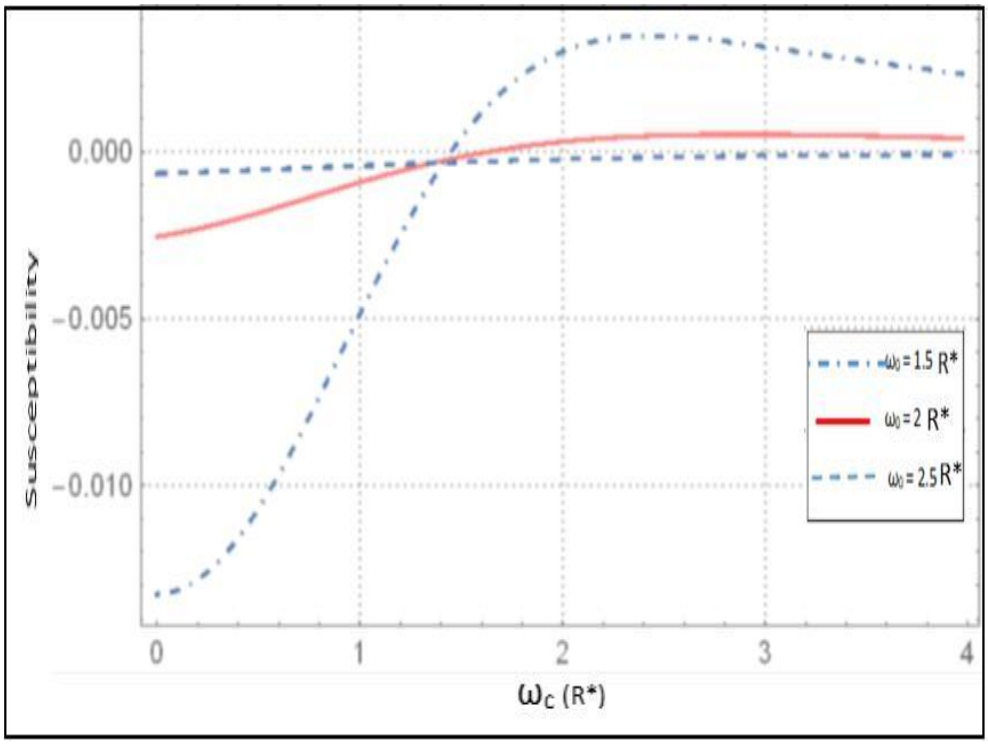

Figure 3.18: Susceptibility vs $\omega_c$with different ω_0 values (ω_0 =2R* for solid line, = 2.5 R* for dashed line, = 1.5 R* for dot dashed) with T= .01 K, F =4.8 R*, θ =60 ^{0}, $\hbar = 1$ $(Rydberg\ units)$.

In Figures (3.19), and (3.20). The effect of θ is presented. Where increasing θ increases the resultant electric field. So, the behavior is similar to that in Figures (3.13), and (3.14). Noticing that in the absence of electric field (θ =0), the change in is smooth and with no peak and χ remains approximately constant in the diamagnetic regime.

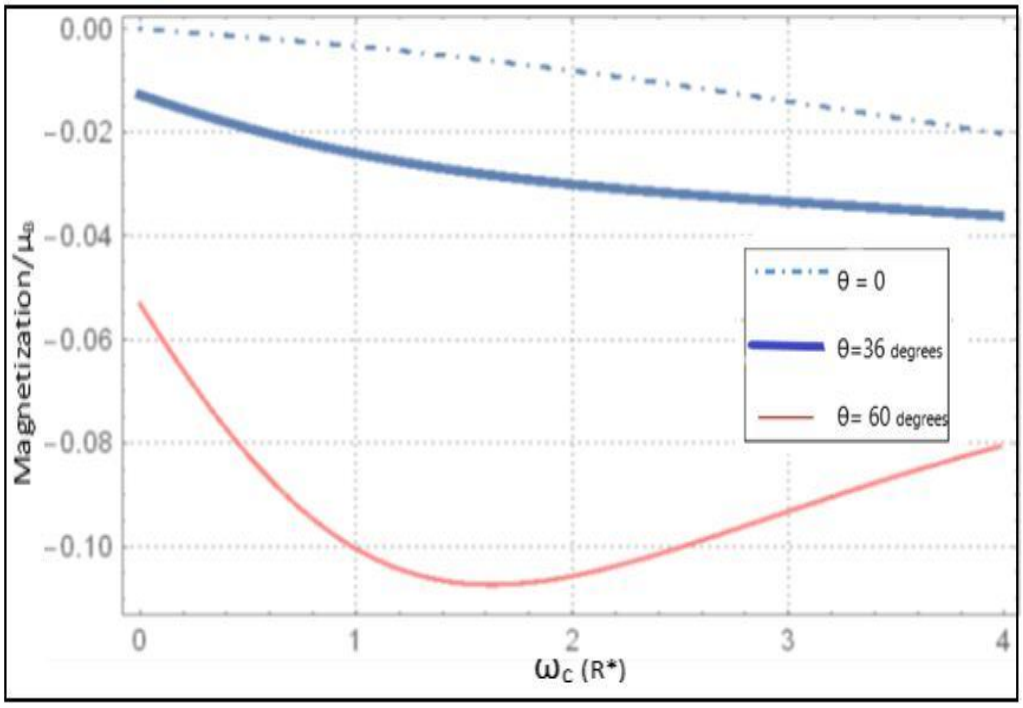

Figure 3.19: Magnetization vs $\omega_c$with different θ values (θ =60 ^{0} for solid line, = 36 ^{0}for thick line, = 0^0 for dot dashed) with T= .01 K, F =4.8 R*, ω_0 =2R*, $\hbar = 1$ ($Rydberg\ units$).

For quite high magnetic field range: (ω_c: 1.5R* - 4 R*), the χ increases as the tilt angle (θ) increases. The increment in (θ) enhances the strength of the electric field, and thus, decreases the donor energy. In this case M decreases while χ increases.

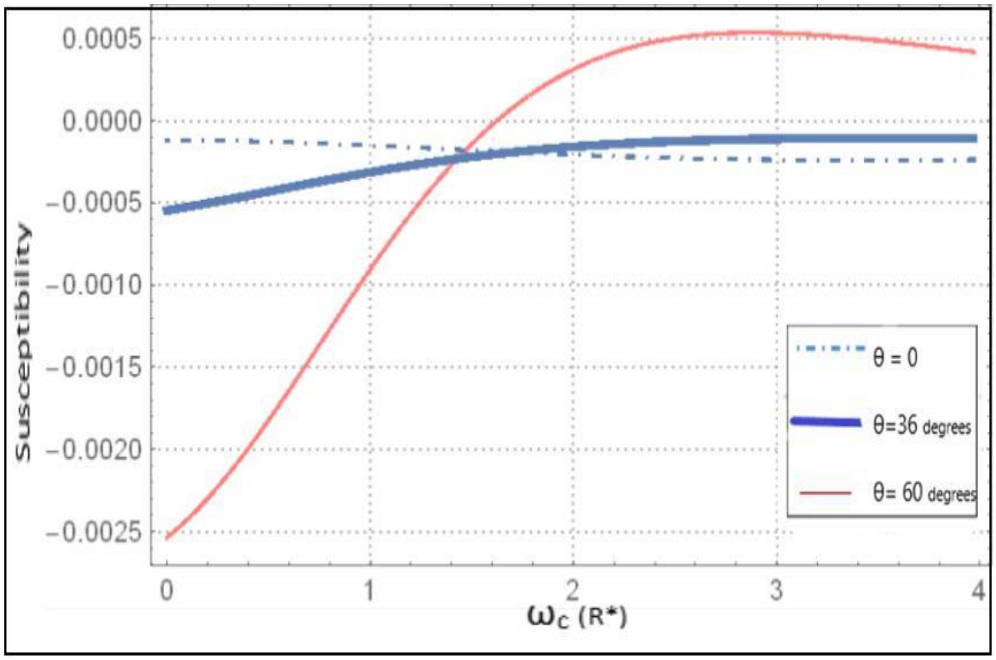

Figure 3.20: Susceptibility vs ω_c with different θ values (θ =60 ^{0} for solid line, = 36 ^{0} for thick line, = 0^0 for dot dashed) with T = .01 K, F =4.8 R*, ω_0 =2R*, $\hbar = 1$ ($Rydberg\ units$).

Again, θ can control the sign of χ.

In addition, we plotted M and χ against ω_c in the presence and absence of impurity, and the results are presented in Figures (3.21), and (3.22) respictively. When the impurity exists, the M changes from decreasing into increasing (transition from diamagnetic regime to paramagnetic one at about ω_c= 1.6 R*), but in the absence of impurity, M decreases until it reaches saturation at about ω_c = 2.5 R* where χ became constant.

The attractive Coulomb energy term due to the donor impurity, reduces the

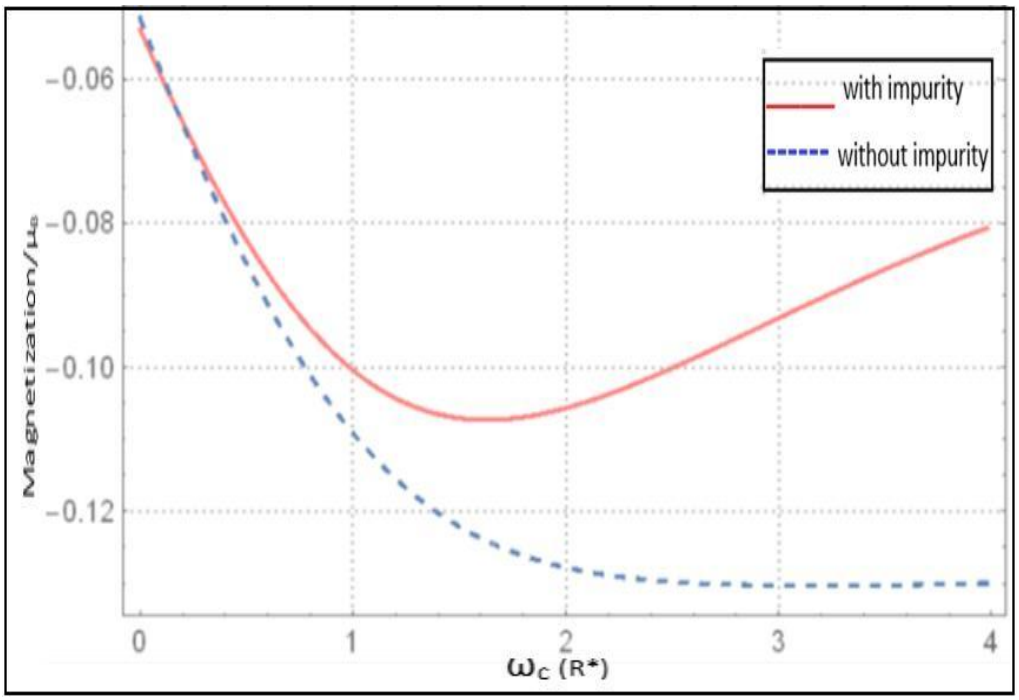

Figure 3.21: Magnetization vs ω_c with the presence/absence of impurity (solid/dashed) with T= .01 K, F =4.8 R*, ω_0 =2R*, θ = 60 ^{0}, $\hbar = 1$ $(Rydberg\ units)$.

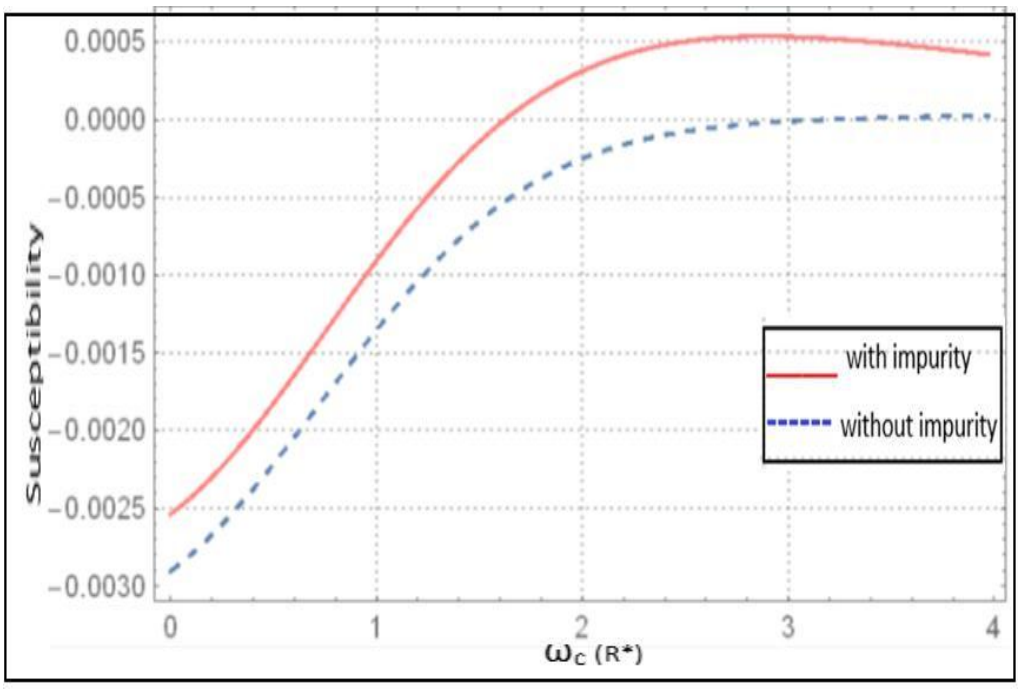

Figure 3.22: Susceptibility vs ω_c with the presence/absence of impurity (solid/dashed) with T= .01 K, F = 4.8 R*, ω_0 = 2R*, θ = 60 ^{0}, $\hbar = 1$ $(Rydberg\ units)$.

energy of the electron in the QD, which results in reducing the magnetization of the QD, (Figure 3.21).

The donor impurity decreases the magnetization as we explained in Figure (3.21), and in this case, the magnetic susceptibility enhances as the magnetic field increases. (Figure 3.22).

We have also studied the effects of RSOI. The effects of the presence or ab- sence of RSOI on M and χ are displayed in Figures (3.23), and (3.24), respectively. Considering the strength of coupling; Figures (3.25) and (3.26) show the effect of coupling strength on both M and χ. In weak coupling (α = 20 meV.nm) the transition from diamagnetic to paramagnetic occurs at low $\omega_c$while at higher coupling strength (α = 50 meV.nm) the transition occurs at ω_c = 2R* and after that the effect of high coupling became dominant, since as shown in equation (2.8), the effect of RSOI appears in two places, one with ω_0 and the other with ω_c. For spin up case, M enhances as αincreases. The α effect is clear in $\omega_{eff}$and L_z terms given in equation (2.8).

χ decreases as α increases. The Rashba effect leads to control greatly the χ of the QD material used in the Spintronics nano-devices, (Figure 3.24).

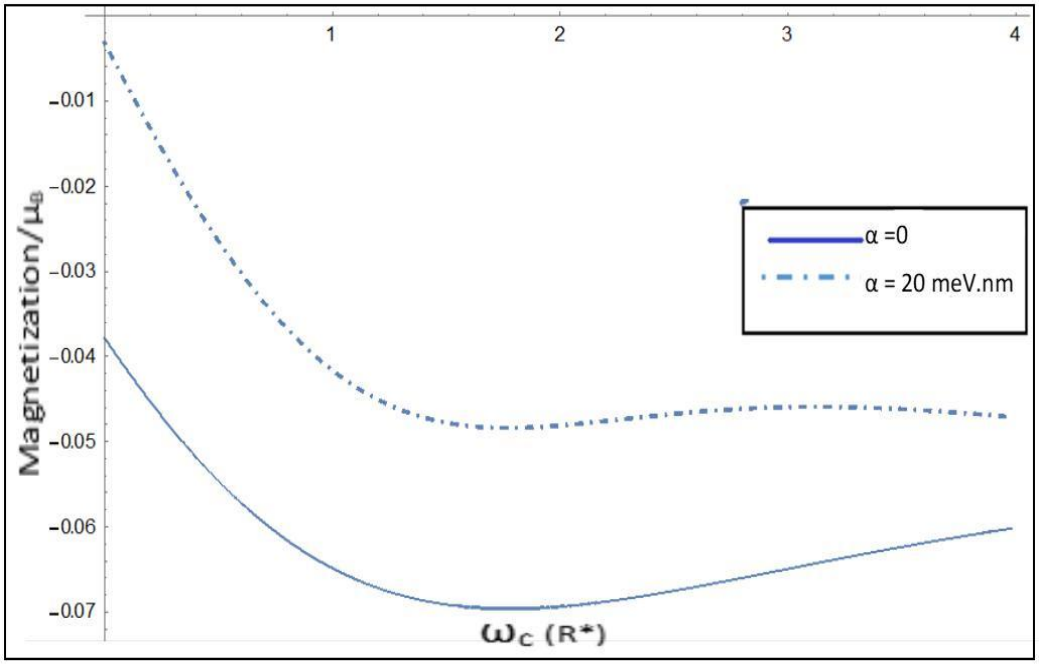

Figure 3.23: Magnetization vs ω_c with the presence/absence of RSOI (solid/dot dashed) with T= .01 K, F =4.8 R*, ω_0 =2R*, θ = 60 ^{0}, $\hbar = 1$ $(Rydberg\ units)$.

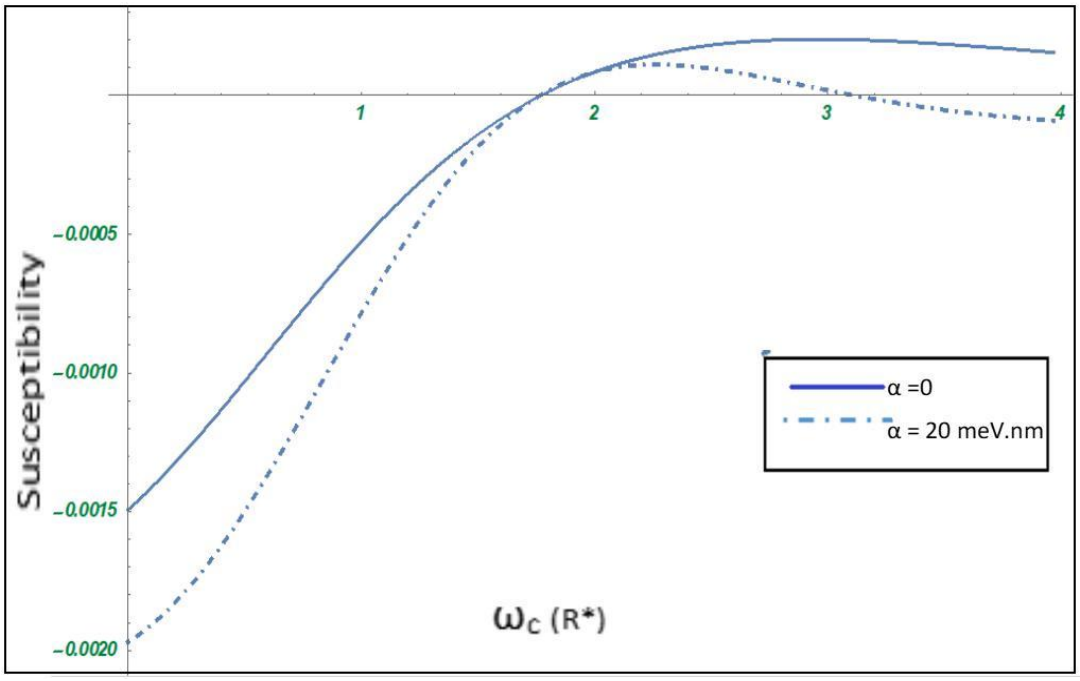

Figure 3.24: Susceptibility vs ω_c with the presence/absence of RSOI (solid/dot dashed) with T= .01 K, F =4.8 R*, ω_0 =2R*, θ = 60 ^{0}, $\hbar = 1$ $(Rydberg\ units)$.

Figure (3.26) shows clearly the effect of changing the Rashba coupling strength on the χ of the QD- material.

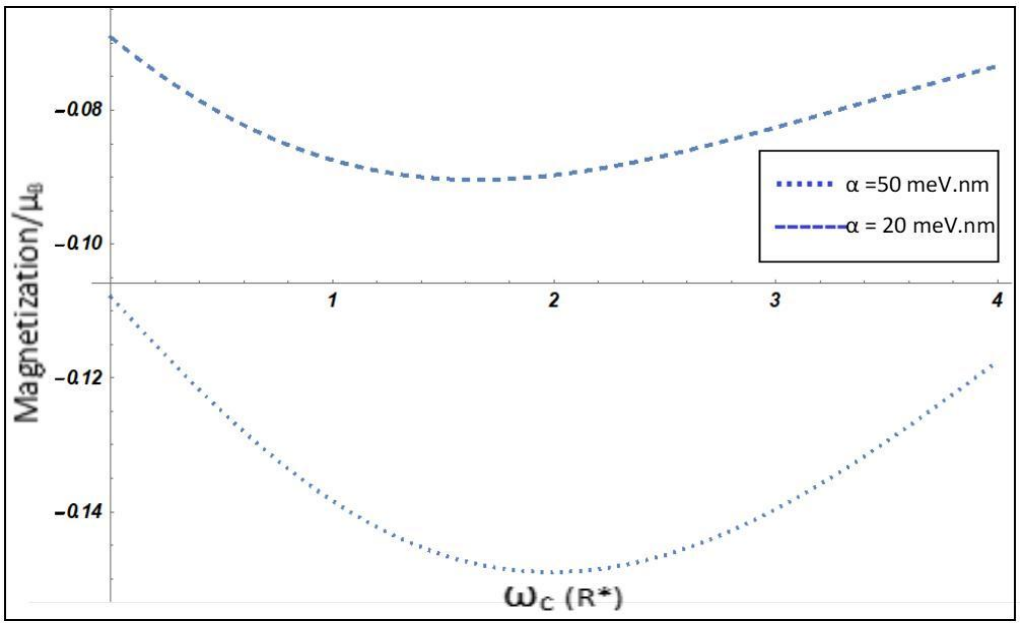

Figure 3.25: Magnetization vs ω_c with different values of RSOI coupling strengths a (a= 20 meV.nm for dashed line, = 50 meV.nm for dotted line) with T= .01 K, F =4.8 R* , ω_0 =2R*, θ = 60 ^{0}, $\hbar = 1$ $(Rydberg\ units)$.

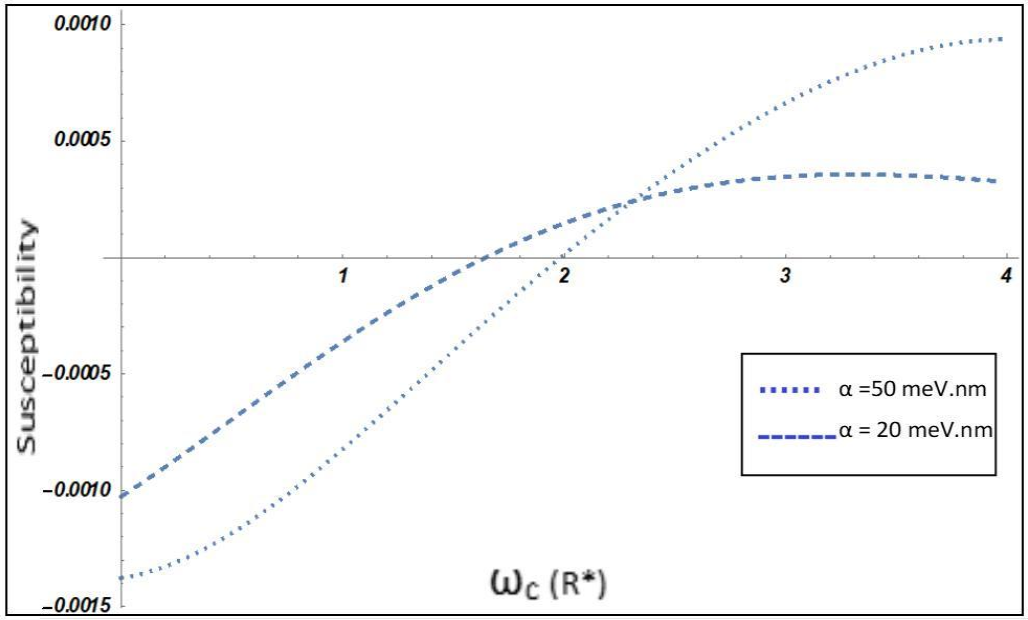

Figure 3.26: Magnetization vs ω_c with different values of RSOI coupling strengths α (α= 20 meV.nm for dashed line, = 50 meV.nm for dotted line) with T= .01 K, F =4.8 R*, ω_0 =2R*, θ = 60 ^{0}, $\hbar = 1$ $(Rydberg\ units)$.

3.5 Heat Capacity

The final step in our work was to calculate the heat capacity for different cases.

The variation of heat capacity as a function of temperature for different values of F are shown in Figure (3.27). In this case, for high values of F, the heat capacity is large, but at certain T (about 90 K) there is intersection and a flip in the behavior, so at high T(T >90 K), the heat capacity is smaller for high electric fields.

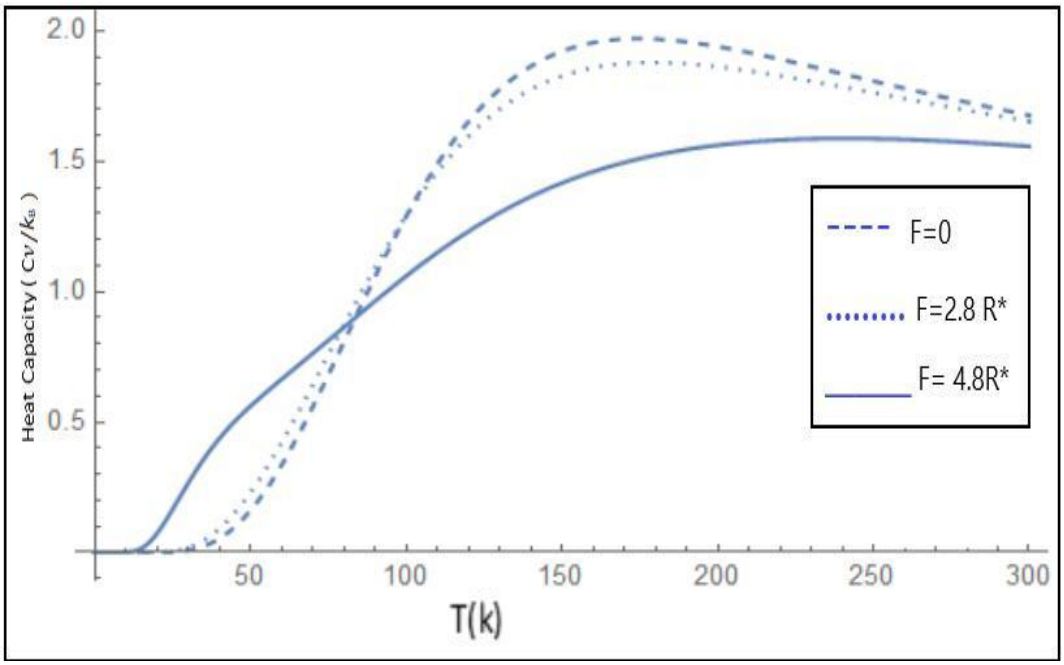

Figure 3.27: Heat Capacity against T with different values of F (F= 0 for solid line, = 2.8 R* for dotted line, = 4.8 R* for dashed line), ω_0 =2R*, wc= 2R* and θ = 60 ^{0}, $\hbar = 1$ $(Rydberg\ units)$.

As the electric field increases, the binding energy of the donor impurity decreases, and in this case, the heat capacity ($C\nu = \frac{d\langle E\rangle}{dT}$), decreases as shown in Figure (3.27).

The effect of RSOI coupling is illustrated in Figure (3.28).

First, as the temperature increases, the heat capacity increases more rapidly for (α= 50 meV.nm) than for (α = 20 meV. nm), then the increase became smooth giving rise to a peak (shoulder). This peak - like structure is known as Schottky anomaly of heat capacity [43].

RSOI sharpens the peak and makes it occur at lower temperature, and that is due to the fact that RSOI rises the degeneracy of states, and so, the energy spacing between levels became smaller, so, it is easier for the electron to be excited to the next higher available level. So, the peak for large a is at lower T than for smaller α.

With the further increase in T, $C\nu$ starts to increase almost linearly until it reaches saturation value of about 1.5 $K_B T$.

This steady increase in $C\nu$ with T is due to the increase in the thermal energy of electrons, which makes more and more states available for thermal excitation.

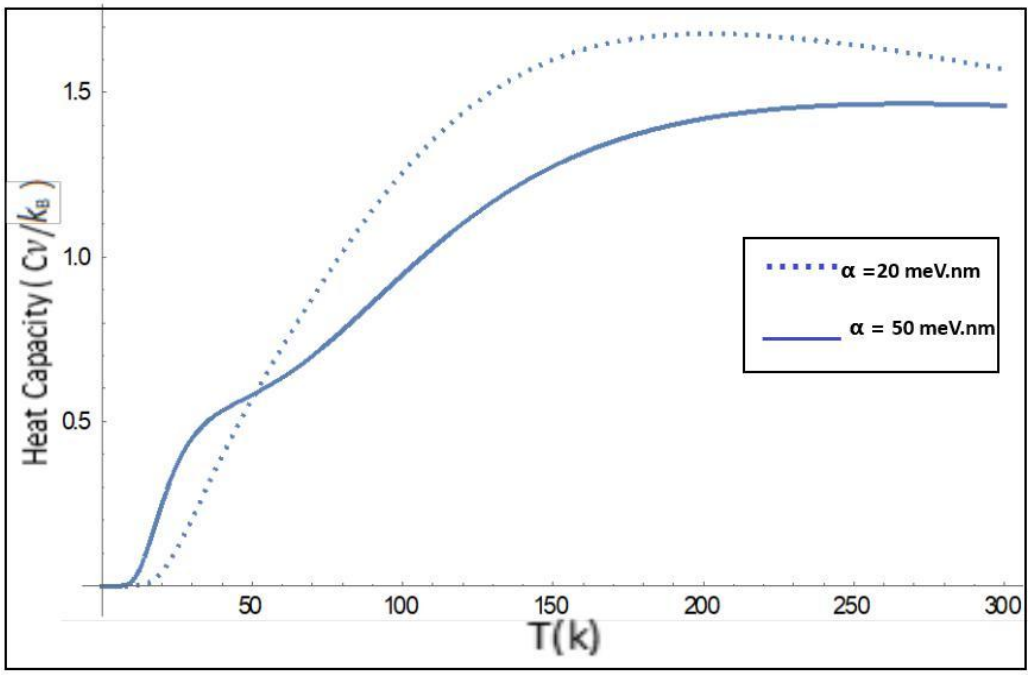

Figure 3.28: Heat Capacity against T with different values of RSOI coupling strengths α (α= 20 meV.nm for dashed line, = 50 meV.nm for dotted line) with F =4.8 R*, ω_0 =2R* and θ = 60 ^{0}, $\hbar = 1$ $(Rydberg\ units)$.

Chapter 4
Conclusion and Future work

In this study, the Hamiltonian of donor impurity in QD had been solved in the presence of magnetic field and tilted electric field, in addition to Rashba Spin Orbit Interaction effect (α and S), and parabolic confinement potential, using exact diagonalization method. We have studied the dependence of the binding energy for our QD as a function of: tilted angle (θ), electric field strength (F), and confinement frequency (ω_0). Our results are in good agreement with reported works.

Moreover, the statistical energy($\langle E \rangle$) spectra and then both Magnetization (M) and Susceptibility (χ) were computed as a function of our controllable parameters (T, F, ω_0, α). It was found that increasing either F or α lowers the values of the statistical energy values, which in turn affects M, making it decreases at lower ω_c and increases at higher ω_c more rapidly, making transition from diamagnetic regime into paramagnetic one at lower value of ω_c. Decreasing temperature diminishes $\langle E \rangle$, and the transition from diamagnetic to paramagnetic is more obvious and faster for lower temperature. But for high values of ω_0 the effect of those parameters is minor, where the influence of ω_0 will be dominant.

As a final step, the influence of F and RSOI on the Heat Capacity (C_v) had been Studied. It was found that with higher F and α , C_v is higher at low temperature, and the situation is reversed for higher values of temperature.

The investigation of magnetic properties and the Spin-Orbit Interaction terms are significant steps in the field of Spintronics. So, In the future, our plan is to continue these research efforts along this line of hot research topics. And we intend to study the effect of more parameters on the magnetic properties of the QD. Entropy is another property that will be considered in the future.

References

[1] Paul Harrison. **Quantum wells**. Wires and Dots, John Wiley&Sons, Chichester, 2005.

[2] Sandip Tiwari, Farhan Rana, Kevin Chan, Leathen Shi, and Hussein Hanafi**. Single charge and confinement effects in Nano-crystal memories**. Applied Physics Letters, 69(9):1232–1234, 1996.

[3] James A. Schwarz, Cristian I Contescu, and Karol Putyera. **Dekker encyclopedia of nanoscience and nanotechnology**, volume 3. CRC press, 2004.

[4] H. Bahramiyan and R. Khordad. **Effect of various factors on binding energy of pyra-mid quantum dot: pressure, temperature and impurity position.** Optical and Quan-tum Electronics, 46(5):719–729, 2014.

[5] YB Xu, SSA Hassan, PKJ Wong, Jian Wu, JS Claydon, YX Lu, Christian Danvad Damsgaard, J. B. Hansen, C. S. Jacobsen, Y. Zhai, et al. **Hybrid spintronic structures with magnetic oxides and heusler alloys**. IEEE Transactions on Magnetics, 44(11): 2959–2965, 2008.

[6] Shu-Shen Li and Jian-Bai Xia. ***Binding energy of a hydrogenic donor impurity in a rectangular parallelepiped-shaped quantum dot: quantum confinement and stark effects*. Journal of applied physics**, 101(9):093716, 2007.

[7] C. Bose and C. K. Sarkar**. Effect of a parabolic potential on the impurity binding energy in spherical quantum dots**. Physica B: Condensed Matter, 253(3-4):238–241, 1998.

[8] M. Kırak, S. Yılmaz, M S¸ahin, and M. Gencaslan. ***The electric field effects on the binding energies and the nonlinear optical properties of a donor impurity in a spherical quantum dot***. **Journal of applied physics**, 109(9):094309, 2011.

[9] G. Murillo and N Porras-Montenegro. **Effects of an electric field on the binding energy of a donor impurity in a spherical GaAs quantum dot with parabolic confinement.** physica status solidi (b), 220(1):187–190, 2000.

[10] Chayanika Bose. ***Binding energy of impurity states in spherical quantum dots with parabolic confinement***. **Journal of applied physics**, 83(6):3089–3091, 1998.

[11] Jia-Lin Zhu, Jia-Jiong Xiong, and Bing-Lin Gu. **Confined electron and hydrogenic donor states in a spherical quantum dot of gaas-ga 1- x al x as.** Physical Review B, 41(9):6001, 1990.

[12] Shu-Shen Li and Jian-Bai Xia. ***Binding energy of a hydrogenic donor impurity in a rectangular parallelepiped-shaped quantum dot: quantum confinement and stark effects***. **Journal of applied physics**, 101(9):093716, 2007.

[13] N Porras-Montenegro, ST Pe, et al. **Hydrogenic impurities in gaas-(ga, al) as quan-tum dots**. Physical Review B, 46(15):9780, 1992.

[14] R Charrour, M Bouhassoune, M Fliyou, and A Nougaoui. **Magnetic field effect on the binding energy of a hydrogenic impurity in cylindrical quantum dot**. Physica B: Condensed Matter, 293(1-2): 137–143,2000 .

[15] A Sali, J Kharbach, A Rezzouk, and M Ouazzani Jamil. **The effects of polaronic mass and conduction band non-parabolicity on a donor binding energy under the simultaneous effect of pressure and temperature basing on the numerical fem in a spherical quantum dot**. Super lattices and Microstructures, 104:93–103, 2017

[16] P Baser and S Elagoz. **The hydrostatic pressure and temperature effects on hydro-genic impurity binding energies in lattice matched inp/in0. 53ga0. 47as/inp square quantum well**. Superlattices and Microstructures, 102:173–179, 2017.

[17] A John Peter. **The effect of hydrostatic pressure on binding energy of impurity states in spherical quantum dots**. Physica E: Low-dimensional Systems and Nanostruc-tures, 28(3):225–229, 2005.

[18] Fanyao Qu, DR Santos Jr, RB Azevedo, V Lopez´-Richard, and GE Marques. ***Tun-able magnetic property of lateral quantum dot molecules***. **In Journal of Physics: Conference Series**, volume 334, page 012064. IOP Publishing, 2011.

[19] Orion Ciftja. ***Generalized description of few-electron quantum dots at zero and nonzero magnetic fields***. **Journal of Physics: Condensed Matter**, 19(4):046220, 2007.

[20] Kaori Tanaka. **Semiclassical study of the magnetization of a quantum dot.** Annals of Physics, 268(1):31–60, 1998.

[21]A Soylu. **The influence of external fields on the energy of two interacting electrons in a quantum dot**. Annals of Physics, 327(12):3048–3062, 2012.

[22] MJ Karimi and G Rezaei. **Effects of external electric and magnetic fields on the linear and nonlinear intersubband optical properties of finite semi-parabolic quantum dots**. Physica B: Condensed Matter, 406(23):4423–4428, 2011.

[23] Dali Wang, Guojun Jin, Yongyou Zhang, and Yu-qiang Ma. ***Effect of a tilted electric field on the magnetoexciton ground state in a semiconductor quantum dot***. **Journal of applied physics**, 105(6):063716, 2009.

[24] SJ Liang and WF Xie. ***The hydrostatic pressure and temperature effects on a hydro-genic impurity in a spherical quantum dot***. **The European Physical Journal B**, 81(1): 79–84, 2011.

[25] H Akbas, I Erdogan, and O Akankan. **Hydrostatic pressure effects on impurity states in GaAs quantum wells**. Superlattices and Microstructures, 50 (1):80–89, 2011.

[26] Anuja Ghosh and Manas Ghosh. **Role of anisotropy, spatially-varying effective mass, and dielectric constant on self-polarization effect of doped quantum dots in presence of noise**. Superlattices and Microstructures, 104:438–444, 2017.

[27] Mahdi Eshghi, Hussain Mehraban, and Sameer M Ikhdair. **Killingbeck mass spec-trum of heavy quarkonia under the influence of external magnetic and ab flux fields**. arXiv preprint arXiv:1704.00776, 2017.

[28] Faten Bzour, Ayham Shaer, and Mohammad K Elsaid. ***The effects of pressure and temperature on the exchange energy of a parabolic quantum dot under a magnetic field.*** **Journal of Taibah University for Science**, 2017.

[29] Aalu Boda and Ashok Chatterjee. **Transition energies and magnetic properties of a neutral donor complex in a gaussian GaAs quantum dot**. Superlattices and Mi-crostructures, 97:268–276, 2016.

[30] Tatsuki Tojo, Masashi Inui, Ryo Ooi, Kyozaburo Takeda, and Yasuhiro Tokura. ***Ef-fect of isotropy and anisotropy of the confinement potential on the rashba spin–orbit interaction for an electron in a two-dimensional quantum dot system***. **Japanese Jour-nal of Applied Physics**, 56(7):075201, 2017.

[31] Aalu Boda, Bahadir Boyacioglu, Ugur Erkaslan, and Ashok Chatterjee. **Effect of rashba spin–orbit coupling on the electronic, thermodynamic, magnetic and trans-port properties of gaas, inas and insb quantum dots with gaussian confinement**. Phys-ica B: Condensed Matter, 498:43–48, 2016.

[32] Nezhat Pournaghavi, Mahdi Esmaeilzadeh, Adib Abrishamifar, and Somaieh Ah-madi. ***Extrinsic rashba spin–orbit coupling effect on silicene spin polarized field effect transistors***. **Journal of Physics: Condensed Matter**, 29(14):145501, 2017.

[33] Jairo Sinova, Dimitrie Culcer, Qian Niu, NA Sinitsyn, **T Jungwirth, and AH Mac-Donald. Universal intrinsic spin hall effect.** Physical review letters, 92(12):126603, 2004.

[34] Tsung-Min Hwang, Wen-Wei Lin, Wei-Cheng Wang, and Weichung Wang. ***Numerical simulation of three-dimensional pyramid quantum dot***. **Journal of computational physics**, 196(1):208–232, 2004.

[35] HT Johnson, LB Freund, CD Akyuz,¨ and A Zaslavsky. ***Finite element analysis of strain effects on electronic and transport properties in quantum dots and wires***. **Journal of applied physics**, 84(7):3714–3725, 1998.

[36] R Khordad and N Fathizadeh. **Simultaneous effects of temperature and pressure on diamagnetic susceptibility of a shallow donor in a quantum antidot**. Physica B: Condensed Matter, 407(8):1301–1305, 2012.

[37] A Vanitha and AJ Peter. ***Effects of applied magnetic field on the infrared transitions between hydrogenic states in a corrugated quantum well.*** **The European Physical Journal B-Condensed Matter and Complex Systems**, 73(4):547–553, 2010.

[38] Mohammad El-Said. **Effects of applied magnetic field on the energy levels of shal-low donors in a parabolic quantum dot**. Physica B: Condensed Matter, 202(1-2): 202–206, 1994.

[39] Zaiping Zeng, Christos S Garoufalis, and Sotirios Baskoutas. ***Combination effects of tilted electric and magnetic fields on donor binding energy in a GaAs/AlGaAs cylindrical quantum dot***. **Journal of Physics D: Applied Physics**, 45(23):235102, 2012.

[40] A Chafai, I Essaoudi, A Ainane, F Dujardin, and R Ahuja. **Tuning the binding energy of on-center donor in cdse/znte core/shell quantum dot by spatial parameters and magnetic field strength**. Physica E: Low-dimensional Systems and Nanostructures, 94:96–99, 2017.

[41] A Sivakami and M Mahendran. **Hydrostatic pressure and temperature dependence of correlation energy in a spherical quantum dot**. Superlattices and Microstructures, 47(4):530–537, 2010.

[42] Xie Wen-Fang. **Ground state of a two-electron quantum dot with a gaussian confin-ing potential.** Chinese Physics Letters, 23(1):193, 2006.

[43] Sukirti Gumber, Manoj Kumar, Pradip Kumar Jha, and Man Mohan. **Thermody-namic behaviour of rashba quantum dot in the presence of magnetic field**. Chinese Physics B, 25(5):056502, 2016.

[44] G Rezaei and S Shojaeian Kish. **Effects of external electric and magnetic fields, hydrostatic pressure and temperature on the binding energy of a hydrogenic impurity confined in a two-dimensional quantum dot**. Physica E: Low-dimensional Systems and Nanostructures, 45:56–60, 2012.

[45] Faten Bzour, Mohammad K Elsaid, and Khaled F Ilaiwi. ***The effects of pressure and temperature on the energy levels of a parabolic two-electron quantum dot in a magnetic field***. **Journal of King Saud University-Science**, 2017.

[46] D Sanjeev Kumar, Soma Mukhopadhyay, and Ashok Chatterjee. ***Magnetization and susceptibility of a parabolic InAs quantum dot with electron–electron and spin–orbit interactions in the presence of a magnetic field at finite temperature*.** **Journal of Magnetism and Magnetic Materials**, 418:169–174, 2016.

[47] MM Al Shorman, FS Nammas, H Haddad, and AA Shukri. ***Heat capacity and entropy of two electrons quantum dot in a magnetic field with parabolic interaction*.** **Chinese Journal of Physics**, 56(3):1057–1063, 2018.

[48] Siranush Avetisyan Jr. **Fock-darwin states of anisotropic quantum dots with rashba spin-orbit coupling**. 2012.

[49] Marieke van Beest. **Fock-darwin states for an elliptical spin-orbit coupled quantum well**. 2015.

[50] Ayham Shaer, MOHAMMAD ELSAID, and Musa Elhasan. ***The magnetic proper-ties of a quantum dot in a magnetic field***. **Turkish Journal of Physics**, 40(3):209–218, 2016.

[51] Ayham SHAER, Mohammad K ELSAID, and Musa ELHASAN. ***Magnetization of GaAs parabolic quantum dot by variation method***. **Journal of Physical Science and Application**, 6(2):39–46, 2016.

[52] B Boyacioglu and A Chatterjee. ***Heat capacity and entropy of a GaAs quantum dot with gaussian confinement*.** **Journal of applied physics,** 112(8):083514, 2012.

[53] Hayk T Ghaltaghchyan, Edward M Kazaryan, and Hayk A Sarkisyan. **Diamag-netism in the cylindrical quantum dot with parabolic confinement potential**. xxx, (3): 20–24, 2016.

[54] KOOLE, Rolf, et al. **Size effects on semiconductor nanoparticles. In:** ***Nanoparticles***. Springer, Berlin, Heidelberg, 2014. p. 13-51.

[55] BULUTA, Iulia; ASHHAB, Sahel; NORI, Franco. **Natural and artificial atoms for quantum computation**. *Reports on Progress in Physics*, 2011, 74.10: 104401.

[56] https://www.semanticscholar.org/paper/Spins-in-few-electron-quantum-dots-Hanson/13c2de3fd55e54c674186583a9e48b745d5e3070/figure/9.

[57] https://web.stanford.edu/group/MarcusLab/research.html

[58]SAITO, Yoshiaki, et al. ***Spin-based MOSFET and its applications.*** **Journal of the Electrochemical Society**, 2011, 158.10: H1068-H1076.

Appendix A

The pressure and temperature dependent electron effective mass and static dielectric constant and Rydberg Units

$$m^*(P,T) = \left[1 + 7.51\left(\frac{2}{E_g^{\Gamma}(P,T)} + \frac{1}{E_g^{\Gamma}(P,T)+0.341}\right)\right]^{-1} m_0 \quad \text{(A.1)}$$

$$\epsilon_r\ (P,T) = \begin{cases} 12.47\exp(-1.73\times10^{-3}P)\exp[9.4\times10^{-5}(T-75.6)] & \text{for T} < 200\ \text{K} \\ 13.18\exp(-1.73\times10^{-3}P)\exp[20.4\times10^{-5}(T-300)] & \text{for T} \geq 200\ \text{K} \end{cases} \quad \text{(A.2)}$$

$$E_g^{\Gamma}(P,T) = \left[1.519 - 5.405\times10^{-4}\frac{T^2}{T+204}\right] + bP + cP^2 \quad \text{(A.3)}$$

Where m_0 is the free electron mass, $E_g^{\Gamma}(P,T)$ is the pressure and temperature dependent energy band gap for GaAs quantum dots at Γ point,

b= 1.26×10^{-1}eV GPa^{-1} and c = -3.77×10^{-3}eV GPa^{-2}.

The effective Rydberg in term of pressure and temperature is used as the energy unit.

$$R_y^*(P,T) = \frac{e^2}{2\epsilon(P,T)a_B^*(P,T)} \quad \text{(A.4)}$$

Where $a_B^*(P,T)$ is the effective Bohr radius which given as:

$$a_B^*(P,T) = \frac{\epsilon(P,T)\hbar^2}{m^*(P,T)e^2} \quad \text{(A.5)}$$

Finally, the effective Rydberg can be written as: (A.6)

$$R_y^*(P,T) = \frac{e^4 m^*(P,T)}{2\left(\epsilon(P,T)\right)^2\hbar^2} \quad \text{(2.14)}$$

Appendix B

Exact Diagonalization Method

The main steps that were followed to diagonalize our Hamiltonian matrix element given in equation 2.8.

First, considering the Known eigenvalue formula:

$$\widehat{H}\,|\,\Psi\,\rangle = E\,|\,\Psi\,\rangle \tag{B.1}$$

where:

$$|\,\Psi\,\rangle = \sum_{n,m} |\,\Psi_{\,nm}\rangle \tag{B.2}$$

where $\Psi_{\,nm}$ as defined in equation 2.14

Then, multiplying both sides of equation B.1 by $\langle\Psi_{n'm'}\,|$ and using:

$$\langle\Psi_{n'm'}|H|\Psi_{nm}\rangle = \sum_{nm} H_{nm} \tag{B.3}$$

$$\langle\Psi_{n'm'}|\Psi_{nm}\rangle = \delta_{nn'}\delta_{mm'} \tag{B.4}$$

and,

$$\langle E_{nm}\rangle = \langle\Psi_{n'm'}|\widehat{H}|\Psi_{nm}\rangle \tag{B.5}$$

We get:

$$\sum_{nm} H_{nm} = E_{nm}\sum_{nm}\langle\Psi_{n'm'}|\Psi_{nm}\rangle = E_{nm}\delta_{nn'}\delta_{mm'} \tag{B.6}$$

The integral form of the previous equation is:

$$E_{nm} = \int_{-\infty}^{\infty} \Psi \hat{H} \Psi \mathrm{dV} \tag{B.7}$$

Then diagonalizing matrix by:

$$\sum_{nm} \left[H_{nm,n'm'} - E_{nm} \delta_{nn'} \delta_{mm'} \right] = 0 \tag{B.8}$$

Then, the secular characteristic equation is:

$$Det \left[H_{nm,n'm'} - E_{nm} \delta_{nn'} \delta_{mm'} \right] = 0 \tag{B.9}$$

جامعة النجاح الوطنية

كلية الدراسات العليا

تأثيرات المجالين المغناطيسي والكهربائي على الخصائص المغناطيسية لنقطة كمية من زرنخيد الجاليوم المحصورة بجهد قطعي

اعداد

امال جودت نايف الدراوشة

اشراف

أ.د. محمد السعيد

قدمت هذه الأطروحة استكمالاً لمتطلبات الحصول على درجة الماجستير في الفيزياء، بكلية الدراسات العليا، في جامعة النجاح الوطنية، نابلس–فلسطين.

2018

تأثيرات المجالين المغناطيسي والكهربائي على الخصائص المغناطيسية لنقطة كمية من زرنخيد الجاليوم المحصورة بجهد قطعي

اعداد

امال جودت نايف الدراوشة

اشراف

أ.د.محمد السعيد

الملخص

قمنا بدراسة تأثير المجالين المغناطيسي والكهربائي على الخصائص الحرارية لنقطة كمية من GaAs عن طريق حساب مستويات الطاقة لهذه النقطة باستخدام طريقة حساب قطرية المصفوفة. وتم حساب طاقة الربط للشائب وكيفية تغيرها مع تغيير العوامل المتغيرة للنقطة الكمية.

تم استخدام مستويات الطاقة في حساب التمغنط للنقطة الكمية ودراسة تأثير كل من قوة المجال الكهربائي ودرجة الحرارة وتردد القطع ووجود الشائب على كل من مستويات الطاقة والتمغنط والنفاذية المغناطيسية والحرارة النوعية لهذه النقطة.

بالاضافة الى ذلك، تم دراسة تأثير (الرشبا المغزلي) على الخصائص المغناطيسية للنقطة الكمية، حيث أن لهذا العامل دور مهم في علم الالكترونيات المعتمدة على غزل الالكترون "spintronics".

وكانت النتيجة ان وجود المجال الكهربائي وتغيير زاوية ميلانه، المجال المغناطيسي، درجة الحرارة، تردد الحصر، بالإضافة الى تأثير الرشبا تؤثر على الخصائص المغناطيسية للنقطة الكمية، حيث تتغير الطبيعة المغناطيسية للمادة بتغيير قيم هذه المتغيرات. كما أن الحرارة النوعية للنقطة الكمية تتأثر بتغيير قيم هذه المتغيرات.

وكانت النتائج التي حصلنا عليها متوافقة بشكل جيد مع نتائج منشورة سابقا.